Journal of Hydrology 615 (2022) 128668

Contents lists available at ScienceDirect

Journal of Hydrology

journal homepage: www.elsevier.com/locate/jhydrol

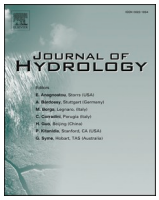

Research papers

Global-scale characterization of streamflow extremes

Sai Kiran Kuntla [a], Manabendra Saharia [a,*], Pierre Kirstetter [b]

[a] Department of Civil Engineering, Indian Institute of Technology Delhi, New Delhi 110016, India
[b] University of Oklahoma, Norman, OK 73019, United States

ARTICLE INFO

This manuscript was handled by Emmanouil Anagnostou, Editor-in-Chief.

Keywords:
Catchment
Floods
Flood characterization
Geomorphology
Streamflow extremes
Unit peak discharge

ABSTRACT

The increasing risk of floods across the globe needs focused attention because of the extensive damage to human lives and economy. A comprehensive understanding of its causative factors is of vital importance. Yet catchment characterization studies are generally limited to case studies or regional domains. A comprehensive global characterization is currently unavailable, which requires collecting and collating a large number of datasets over vast areas. This study embraces large-sample data-driven science as a new paradigm to characterize streamflow extremes by utilizing global datasets of physiographic explanatory variables that could explain various facets of extreme streamflows. Along with the spatial and temporal variations of high streamflow extremes, their correlation with various catchment characteristics such as geomorphology, meteorology, climatology, landcover, lithology, etc. were examined. The multidimensional relationships between the streamflow extremes and catchment characteristics were modeled using a Random Forest approach and combined with an interpretable machine learning framework to identify the most dominant factors in varying climate classes. Interpretation with SHAP (SHapley Additive exPlanations) reveals that meteorological variables are the most influential variables across the climatic classes. However, the variables and their influences change among different climatic classes. Moreover, different geomorphological variables come into dominance across climatic classes (such as basin relief in warm temperate and drainage texture in arid climates). Overall, the insights from the study could play a crucial role in predicting the unit peak discharge at ungauged stations from the known catchment characteristics. Moreover, these findings can also play a crucial role in formulating risk management strategy.

1. Introduction

Extremes are, by definition, rare events. These event values would be above (or below) a threshold value close to the upper (or lower) ends of the range of observed values of the variable (Seneviratne et al., 2012). High streamflow extremes (HSE) are of great importance, considering their ability to cause abrupt damage to lives, livelihood, infrastructure, and the environment. Besides, previous studies have shown an increasing trend in HSE in many parts of the world, such as North America (Dethier et al., 2020), Northern Australia (Zhang et al., 2016), United Kingdom (Hannaford and Marsh, 2008). Besides, flood risk is expected to increase in the future worldwide (Arnell and Gosling, 2016; Winsemius et al., 2016). Hence, understanding the relationship between HSE and its causative drivers is of utmost importance to reduce their adverse effects (Blöschl et al., 2017; Gudmundsson et al., 2019; Mallakpour and Villarini, 2015).

Trends in extreme rainfall might not fully describe the observed patterns in extreme streamflow trends (Huang et al., 2021; Ivancic and Shaw, 2015). Understanding the relationship between catchment characteristics and HSE globally is difficult because it demands reliable and spatially representative time series data as well as data on possible explanatory variables related to meteorology, climatology, geomorphology, and other catchment features. Existing literature confirms that various geomorphological, climatological, and meteorological drivers impact flooding (Ahn and Merwade, 2016; Al-Rawas and Valeo, 2010; Costa, 1987; Gaume et al., 2009; Marchi et al., 2010; Norbiato et al., 2009; Saharia et al., 2017b). For instance from studying a few largest floods over the continental United States, Costa (1987) concludes that the rain duration and intensity, basin physiography, and geology are primary factors in stimulating runoff. While Saharia et al. (2017a) note that the intense monsoon thunderstorms and steep terrain cause the fastest responding events in the arid Southwest United States. Lun et al. (2021) assess the process controls of flood moments across Europe, examining various catchment-scale characteristics such as precipitation, air temperature, soil moisture, evaporation, aridity, and topography. At the same time, Norbiato et al. (2009) observed that soil properties and

* Corresponding author.

https://doi.org/10.1016/j.jhydrol.2022.128668
Received 16 April 2022; Received in revised form 8 October 2022; Accepted 10 October 2022
Available online 9 November 2022

geology are among the catchment variables driving the spatial variability of the runoff coefficient and that the mean annual precipitation is the primary driver over 14 eastern Italian Alps catchments. However, existing studies focusing on the characterization of catchments and their floods are primarily limited to the basin- or regional scales, or at most to the continental scale (Marchi et al., 2010). Most existing studies have focused on Europe and the North American continents and have only considered limited factors to characterize catchments (Ahn and Merwade, 2016; Lun et al., 2021; Marchi et al., 2010; Stein et al., 2021).

Due to the diversity in catchments worldwide, unraveling the catchment characteristics associated with extreme floods is lacking on a global scale. The existing global databases are sporadic and require significant processing to use together, that could be useful for large-sample and -scale studies. Consequently, it limits our understanding on different factors that influence the HSE globally. Large-scale studies are required to identify the most robust insights on catchment behavior and derive general hydrological principles that can be widely accepted (Addor et al., 2020; Gupta et al., 2014). The importance of large sample studies has been further identified as the foundation of a new paradigm of hydrology, which will contribute toward formulation of new relationships that are hindered by the conventional studies of hydrologic phenomena (Peters-Lidard et al., 2017). A few large-sample and global-scale studies have focused on specific aspects of floods, such as trends and timing (Do et al., 2017; Do et al., 2020a; Gudmundsson et al., 2019; Wasko et al., 2020). But none of them examine how catchment characteristics influence HSE and are limited in terms of the number of geophysical and hydrometeorological explanatory variables that have been included. Moreover, these existing studies usually include catchments with human alterations or anthropogenically-influenced, although anthropogenic alterations significantly impact hydrologic behavior. Thus, there is a need to characterize the least altered catchments at a global scale by utilizing large-sample datasets and a large set of explanatory variables. However, truly pristine catchments are globally sporadic (Hodgkins et al., 2017).

This study takes advantage of advanced computational power and multiple global datasets to lay a foundation for developing a comprehensive understanding of HSE globally and advancing our knowledge in the same area. A robust analysis was performed for finding holistic behavior by utilizing a large number of explanatory variables and by examining relationships between HSE and watershed characteristics. Our understanding of the dominant catchment characteristics of HSE from the existing literature is currently limited. Hence, we also tried to assess the relative importance of multiple catchment characteristics with HSE. In this study, a large sample of 45,932 HSE events in 9,710 catchments spread across the globe is used to characterize HSE in catchments with different characteristics employing a large number of explanatory variables.

2. Data used and methods

2.1. Data

Three unique global archives were used to compute and collate hydrological variables of interest and a large number of climatological and geomorphological variables. Extensive pre-processing was performed to match these datasets. Firstly, the annual peak discharge streamflow index, which describes the maximum daily streamflow value in a year, and a small number of catchment characteristics associated with gauge stations spread across the globe were retrieved from the Global Streamflow Indices and Metadata (GSIM) archive (Do et al., 2017; Gudmundsson et al., 2018). Few studies focusing on flood trends and timings have used this variable from the same dataset (Do et al., 2020a; Wasko et al., 2020). Annual peak discharge is widely used as an indicator of a flood as it allows a straightforward interpretation (Do et al., 2020b; Hall et al., 2015; Stein et al., 2020). Since HSE are the rarest events that belong to the upper tail of the observed values, for each station, only the top 10 percentile annual peak discharges over the entire time series of observations are considered as HSE events. As it is expected that channels in larger catchments will collect and carry larger discharges, in this study, the HSE values are normalized based on their corresponding drainage area resulting in scale-independent comparisons across catchments. This normalized value called unit peak discharge (UPD) is an important index for studying floods in catchments with different characteristics. For instance, O'Connor and Costa (2004) discussed how catchments producing high unit peak discharge are distributed spatially in the United States and Puerto Rico, and related this index with specific topographic and climatologic conditions. Gaume et al. (2009), Marchi et al. (2010), and Saharia et al. (2017a) utilized this index in envelope curves to characterize floods in Europe and the continental United States, respectively. These curves establish an upper bound for the floods that may be seen in a particular area. Apart from these studies, Lun et al. (2021) have recently investigated the process controls on spatial patterns of flood moments, including the specific mean annual flood, i.e., the mean of unit peak discharge, across European catchments.

In order to increase the representation of basin geomorphology, a larger set of variables describing basin characteristics were extracted from the Global Distributed Basin Characteristics (GDBC) database with a spatial resolution of 1 km (Shen et al., 2016). The primary products available in the database include basic characteristics such as basin length, basin area, stream order, stream length, etc. A secondary set of geomorphological variables were derived using the primary products available in GDBC, which includes the elongation ratio that describes basin shape, the bifurcation ratio that is considered a useful measure of proneness to flooding (Allaby, 2008), the relief ratio that measures the overall steepness of drainage basin (Schumm, 1956). They allow for investigation of how the size, shape, structure, and other characteristics might impact floods. Lastly, catchment-averaged meteorological and climatic variables were computed from the 1-km resolution WorldClim datasets (Fick and Hijmans, 2017). The WorldClim datasets variables are derived from the monthly rainfall and temperature averages for the years 1970–2000. The GSIM archive contains streamflow indices of about 30,959 gauge stations. Finally, in order to create a high-quality dataset for carefully selected gauging stations, the following criteria were adopted by balancing data availability, geographical location, quality, and compatibility with other datasets:

- Since 1263 gauge stations of GSIM are falling outside the spatial extent of other datasets such as GDBC, these stations were removed from further analysis;
- To ensure the compatibility between the three sources of datasets, the consistency of geographic coordinates of the GSIM gauge stations was tested. It was observed that most gauge stations do not fall exactly on the streamline concerning the GDBC data. An algorithm was developed to derive compatible coordinates among various datasets. 1) The algorithm uses the drainage area specified in the GSIM for every gauge station and performs a nearest neighbor search based on the corresponding GSIM-provided coordinates over the drainage area map of GDBC to verify if it falls on a river network or not. 2) If the geographical coordinates are relocated, the new coordinates will be used. Otherwise, the same old coordinates are used for retrieving the GBDC data, and 3) Shapefiles are developed for all the 9000 + catchments to derive the catchment-averaged climatological variables from the WorldClim, curve number, information on the landcover, Koppen-Geiger climate, lithology, soil, and the number of dams in the catchments.
- Only gauge stations with at least 20 years of data with a minimum of 350 daily values each year were selected to ensure robust data. According to Project team ECA&D & Royal Netherlands Meteorological Institute KNMI (2013), the yearly indices computed with 350 daily values are considered to be more reliable.

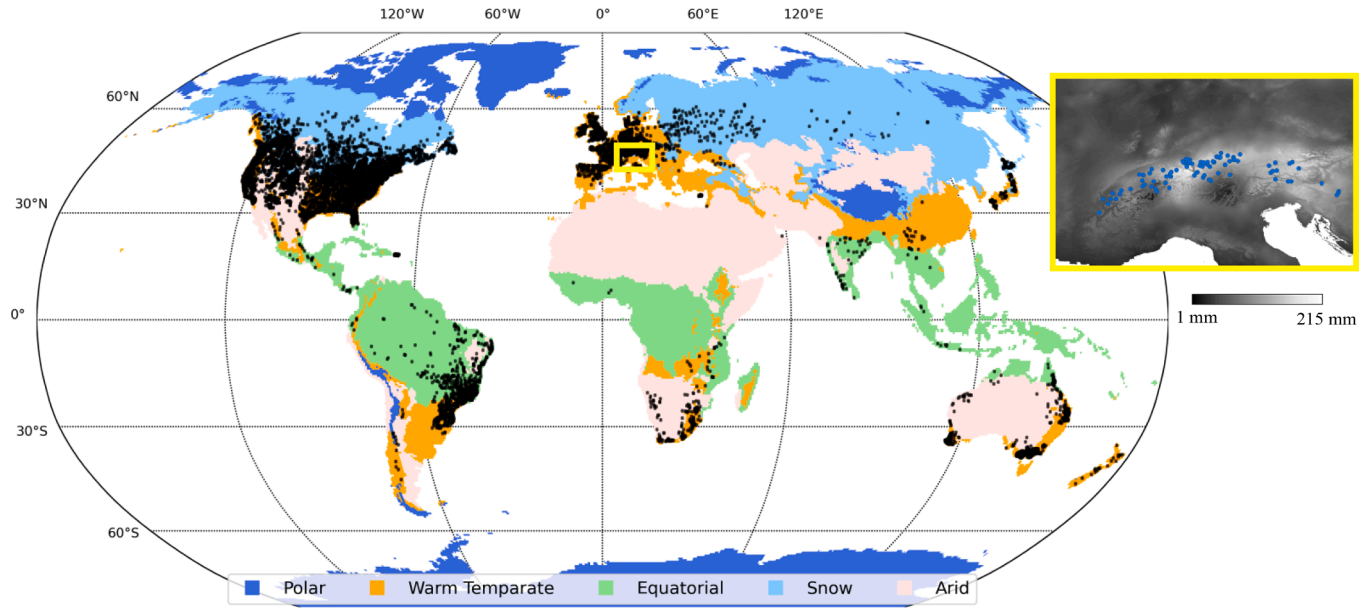

Fig. 1. The geographic location of all the gauge stations and their associated climatic classes used in this study. The yellow box projects a cluster of gauge stations whose catchments are featured with Polar climate, overlayed on a 30-year (1970–2000) average of August month precipitation.

Table 1
Number of gauge stations in various climate regions.

Climate region	Number of gauge stations	Number of HSE events	HSE events/Gauge stations
Polar	113	615	5.44
Warm Temperate	4281	19,822	4.63
Equatorial	569	2107	3.70
Snow	4075	20,459	5.02
Arid	667	2903	4.35
No dominant class	5	26	5.2

- Only GSIM gauge stations whose variable of interest – annual peak discharge – is passing the homogeneity test were utilized in this study. A gauge time series is selected if at least three out of the four tests (the standard normal homogeneity test, the Buishand range test, the Pettitt test, and the von Neumann ratio test) accept the null hypothesis at 99 % level. For more details about the homogeneity test, please refer to Gudmundsson et al. (2018). This step ensures that there is no step-change in the time series of annual peak discharge index through its time period that may be possible due to the change in instrumentation, calibration, or damage of the flow measuring instrument or some other reasons (Gudmundsson et al., 2018). It is extremely important as the time-series data of selected gauge stations is available for at least 20 years and a maximum of 133 years for a station within the period 1883–2015. The number of active gauge stations globally reached a peak in the 1980 s with more than 8000 stations and have reduced since then as shown in Fig. S1.
- In order to work with undisturbed basins, an attempt was made to remove those that may experience significant anthropogenic influence on the hydrologic cycle. Only stations with an upstream area lower than 10,000 km^2 were utilized in this study (Kundzewicz et al., 2005; Svensson et al., 2005). In addition, only those gauge stations whose upstream area is devoid of dams are selected, as these catchments are considered less likely to have been modified. The information on dams is retrieved from the Global Reservoir and Dam (GRanD) database (Lehner et al., 2011). Moreover, catchments that are predominantly covered (i.e., more than 50 percent of its surface area) by the "Settlement" land cover class are also avoided in this study as these catchments would have a considerable anthropogenic influence on its hydrological cycle due to human alterations. This study utilizes the Climate Change Initiative Land Cover (CCI-LC) dataset (https://maps.elie.ucl.ac.be/CCI/viewer/) which is available at a spatial resolution of 300 m.

After these careful selection criteria, 9,710 gauge stations (catchments) are selected in the final database.

2.2. Study area

The spatial distribution of the selected gauge stations is shown in Fig. 1, overlaid on the Köppen-Geiger main climatic classes (Kottek et al., 2006). The dominant class of a basin is identified as the climate class that spreads over more than 50 percent of the drainage area. The number of catchments in each climatic class is tabulated in Table 1, along with the number of HSE events in total as well as per station. The considerable representation of catchments and HSE events from all the primary climatic classes attests to the robustness of this study. Koppen-Geiger is one of the most widely used climate classification systems. It is an efficient way to aggregate climatic conditions defined by multiple variables and their seasonality with a meaningful classification scheme. Kottek et al. (2006) produced the Koppen-Geiger map based on mean monthly temperature and precipitation data for the period 1951 to 2000 from the Climatic Research Unit (CRU) of the University of East Anglia and the Global Precipitation Climatology Centre (GPCC) respectively. The criterion of Koppen-Geiger for the main climates is provided in Table A1 in Appendix. The highest number of catchments are located in the warm temperate climatic class. On the other hand, the lowest number of catchments belong to the polar climatic class. As expected, North America and Europe are densely instrumented compared to other

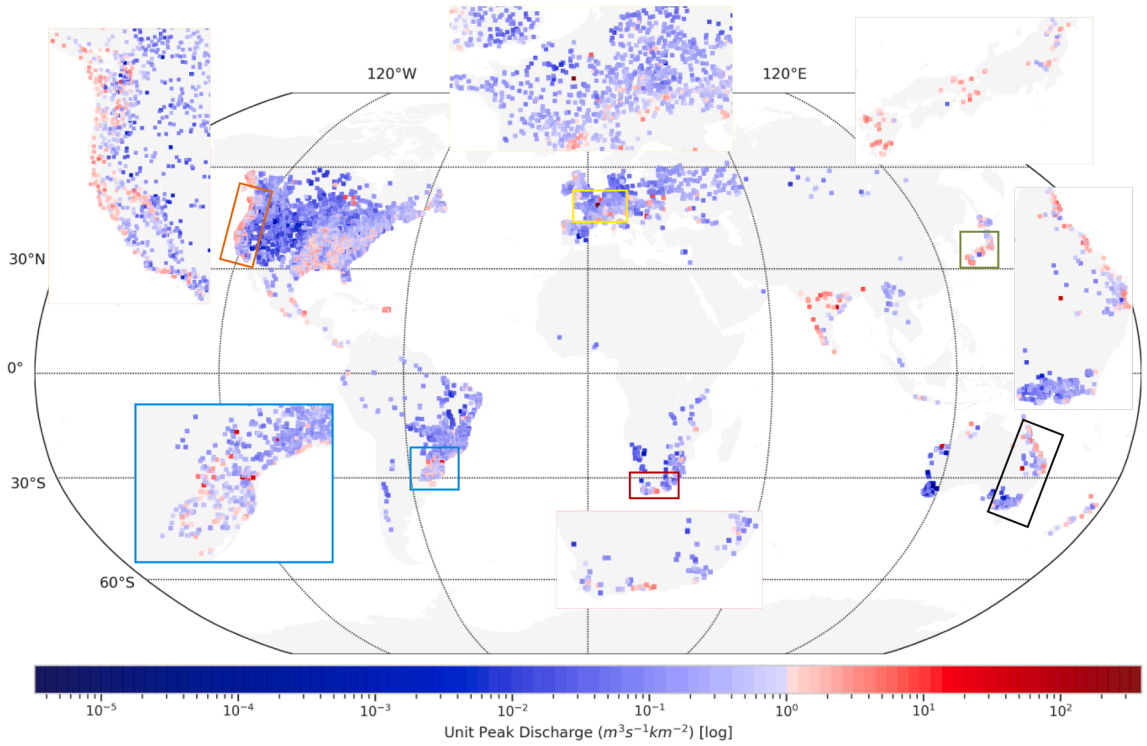

Fig. 2. Spatial distribution of unit peak discharge for the highest streamflow events recorded over the corresponding gauge stations across the globe.

continents. The final dataset is spatially representative across all main climate classes, which will yield unique insights into hydrologic processes, highlighting the potential of the dataset. The basin averaged values of geomorphological and climatological information from GDBC and WorldClim, are augmented to the database to make the comprehensive catchment characteristics database. The final list of all the explanatory variables from the final dataset, which are being considered in this study is provided in Table A2 in Appendix.

2.3. Methods

The study encompasses the following analyses, detailed in the subsequent sections:

1. Section 3 reports the spatial distribution of UPD for the highest streamflow extreme events across the globe. Furthermore, to explore the ranges of UPD over different climatic regimes, box plots are employed. Besides, Section 3 summarizes the temporal patterns of all the HSE events over different climates in the northern and southern hemispheres.
2. Section 4 links the UPD of HSE events to various geomorphological characteristics of catchments, meteorological and climatological variables in Section 5, and to landcover, soil, and lithology in Section 6. These sections explore the first-order dependencies between HSE events and various characteristics of catchments and the variability in these relationships. Firstly, the spearman correlation is computed between the unit peak discharge of all the HSE events and various explanatory variables in the database to evaluate the monotonic relationship between the two variables. Later, box plots for a few highly correlated geomorphological and climatological variables are inspected. In addition, the boxplots for different landcover, lithology, and soils are also investigated for a quick summary of how these land features can influence the UPD of HSE events. Moreover, envelope curves were employed to describe the relationship between drainage area and unit peak discharge. Envelope curves represent the upper limit or envelope of a given data and were used in hydrology studies to provide graphical summaries of extreme floods in various geographical locations across the world (Castellarin, 2007; Crippen and Bue, 1977; Gaume et al., 2009; Kadoya, 1992; Linsley et al., 1949; Saharia et al., 2017a). A simple power-law formula (Eq. (1)) is used to plot the envelope curves on log–log graphs:

$$Q = \alpha A^{\beta} \tag{1}$$

Here $Q(m^3s^{-1}km^{-2})$ is the UPD, $A(km^2)$ is the contributing drainage area, α is the reduced discharge in $(m^3s^{-1}km^{-2(1+\beta)})$, and β is the scaling coefficient. The reduced discharge can be considered an indicator of the magnitude of streamflow by limiting the dependence of the drainage area on the analysis. The β value can be computed by fitting a regression line between log(Q) and log(A), as suggested by Castellarin (2007). The β value reflects the change rate of unit peak discharge with the change in the drainage area. The lower the deviation of β value from zero, the lower the unit peak discharge change with the drainage area.

3. Section 7 dictates the relative importance of different catchment characteristics on the target variable – here, unit peak discharge of HSE. For this purpose, a random forest machine learning model is trained with 75 % of the events, and its predictions on the remaining 25 % of events are evaluated and interpreted using SHAP (Shapley Additive exPlanations) (Lundberg and Lee, 2017). Random forests was introduced by Breiman (2001). It features reduced risk of overfitting, ability to interpret, capability to find nonlinear relationships based on multiple predictors that are beyond our capability, good performance, and reliable uncertainty estimates makes it advantageous for successful usage of this approach in our study. Subsequently, the random forest model has shown favorable performance in the past hydrological signature predictions (Addor et al., 2018; Booker and Woods, 2014; Stein et al., 2021). Though direct feature importance methods are popular to highlight the most important variables in the model, SHAP interpretation has the added advantage of explaining how each feature influence alongside which features influence the model providing in-depth model analysis. Moreover, the conventional feature importance methods are not

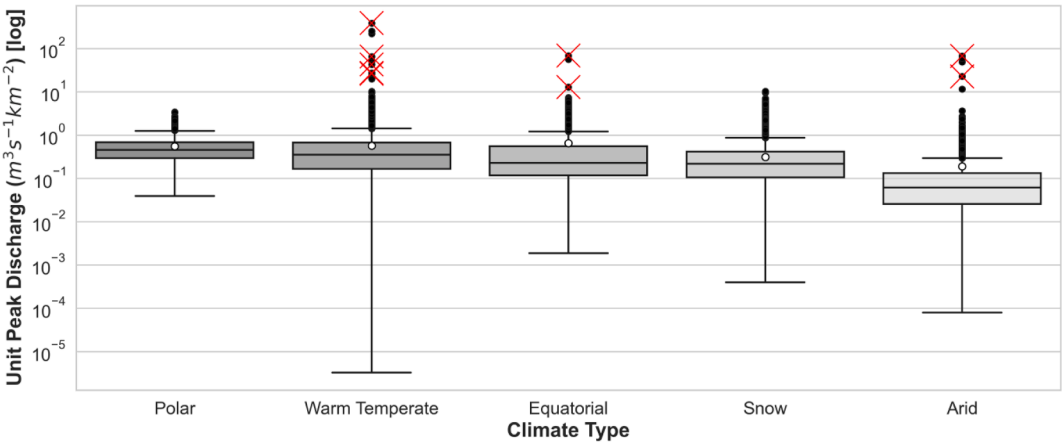

Fig. 3. Box-and-Whisker plot of unit peak discharge for different climatic classes. The box spans the interquartile range in the plot, i.e., the upper and lower ends of the box correspond to the first quartile and third quartiles, respectively. The whiskers are the two vertical lines outside the box extended until the observations' extremes. The median is marked by a horizontal line inside the box, and the mean is plotted with a white circle. The black circles beyond the extremes are considered outliers at a distance of more than 1.5 times the interquartile range. The red cross marks correspond to the top ten catchments in terms of high unit peak discharge values.

suitable for datasets with correlated features such as the one developed for this study (Degenhardt et al., 2019; Dormann et al., 2013). SHAP not only overcomes the problem of multicollinearity but also considers potential synergistic interactions between variables (Lundberg et al., 2020). These features of SHAP make it a powerful interpreter and have recently led to successful application in many fields, including water quality assessment (Wang et al., 2021; Wang et al., 2022).

The SHAP summary plot combines feature importance with feature effects. Each point on the summary plot is a Shapley value for a feature and an instance. The Shapley value is the (weighted) average marginal contribution of a feature value across all possible coalitions (Shapley, 1953). The mean absolute value of shapley values over different instances for the given feature gives the overall importance of the corresponding feature on the target variable - UPD. Overall, the SHAP summary plot demonstrates:

- Feature importance – the order of the features along the y-axis is based on their importance in descending order. The higher (lesser) the absolute mean value of SHAP values provided on the right side of the features name in the plot, the higher (lesser) its relative importance.
- Impact – the horizontal location of the dots depicts the intensity of its influence on predictions. Zero values on the x-axis indicate no impact, and positive (negative) values towards the rights (left) side indicate positive (negative) impact.
- Original value- the color of the dots represents the values of the corresponding features if it is high (red) or low (blue) for that observation in the dataset.
- Correlation- the combined observations of the distribution of dots along the x-axis and their color describe the correlation of the features with the target variable.

3. Spatial and temporal distribution of the HSE events across the globe

Unit peak discharge provides the advantage of allowing the comparison of flooding characteristics across a wide variety of spatial scales. Fig. 2 presents the spatial distribution of UPD of the highest streamflow extreme event recorded over the respective gauge stations across the globe from the database. Similar to the floods in continental United States and Europe that were examined by Saharia et al. (2017a), Marchi et al. (2010), and Gaume et al. (2009), it is observed that the highest UPDs occur over mountainous terrain along oceans, as exemplified by the Cevennes-Vivarais Mediterranean region in France, the West Coast of the continental United States, the coast of western provinces of British Columbia and Yukon in Canada, the west coast of the Canadian island of Newfoundland, the Hidalgo region of Mexico, the northeast region of the Great Dividing Range in Australia, windward side of Cape fold mountains range in South Africa and India's Western Ghats region. In contrast, the unit peak discharge is comparatively low on the leeward side along the Andes Mountains range nearer to the South Pacific Ocean, the leeward side of the Australian Alps in Australia, and the leeward side of the Drakensberg Mountain range in Africa, as expected. Moreover, from the preliminary observations of the database and spatial patterns in Fig. 2, it is observed that many catchments in North and South America having high UPD values belong to the Warm Temperate climate type and are predominantly covered by agriculture and forest landcover. Argentina witnesses some of the most intense mesoscale convective systems on Earth. A field campaign known as RELAMPAGO-CACTI highlighted how deep convection frequently initiates in this region, especially along the complex terrain of Sierras de Córdoba and Andes, and often grows rapidly upscale into dangerous storms resulting in intense flash flooding (Pal et al., 2021). Besides, the geomorphologic characteristics of large parts of its territory make Argentina highly vulnerable to floods. For instance, many of the fluvial systems of the country are connected to mountain environments, such as the Pampean and Cordillera Ranges, along with the Sub-Andean and Eastern Cordillera Ranges, which receive intense and concentrated rainfall during the summertime leading to flash floods in these rivers (Latrubesse and Brea, 2009). Interestingly, most of the European catchments with high UPDs are also dominantly covered by forest or agricultural landcover. Importantly, most of these catchments are of small size. Marchi et al. (2010) reported that a few of the most extreme flash floods and their characteristics across Europe are attributed to small catchment areas. Besides, Brebbia and Katsifarakis (2007) note that the geo-hydrological conditions of heavy rainfall combined with steep slopes and deep valleys in small Mediterranean catchments produce higher UPD. The possible reasons for high UPDs in forest and agriculture dominated catchments is explained in detail in Section 6.

At the same time, Indian catchments display among the highest UPDs and belong to the Equatorial climatic class. They receive very high rainfall due to synoptic scale monsoon disturbances during July and August, with 80 percent of the annual rainfall occurring during the southwest monsoon rainfall from June to September. Besides, these

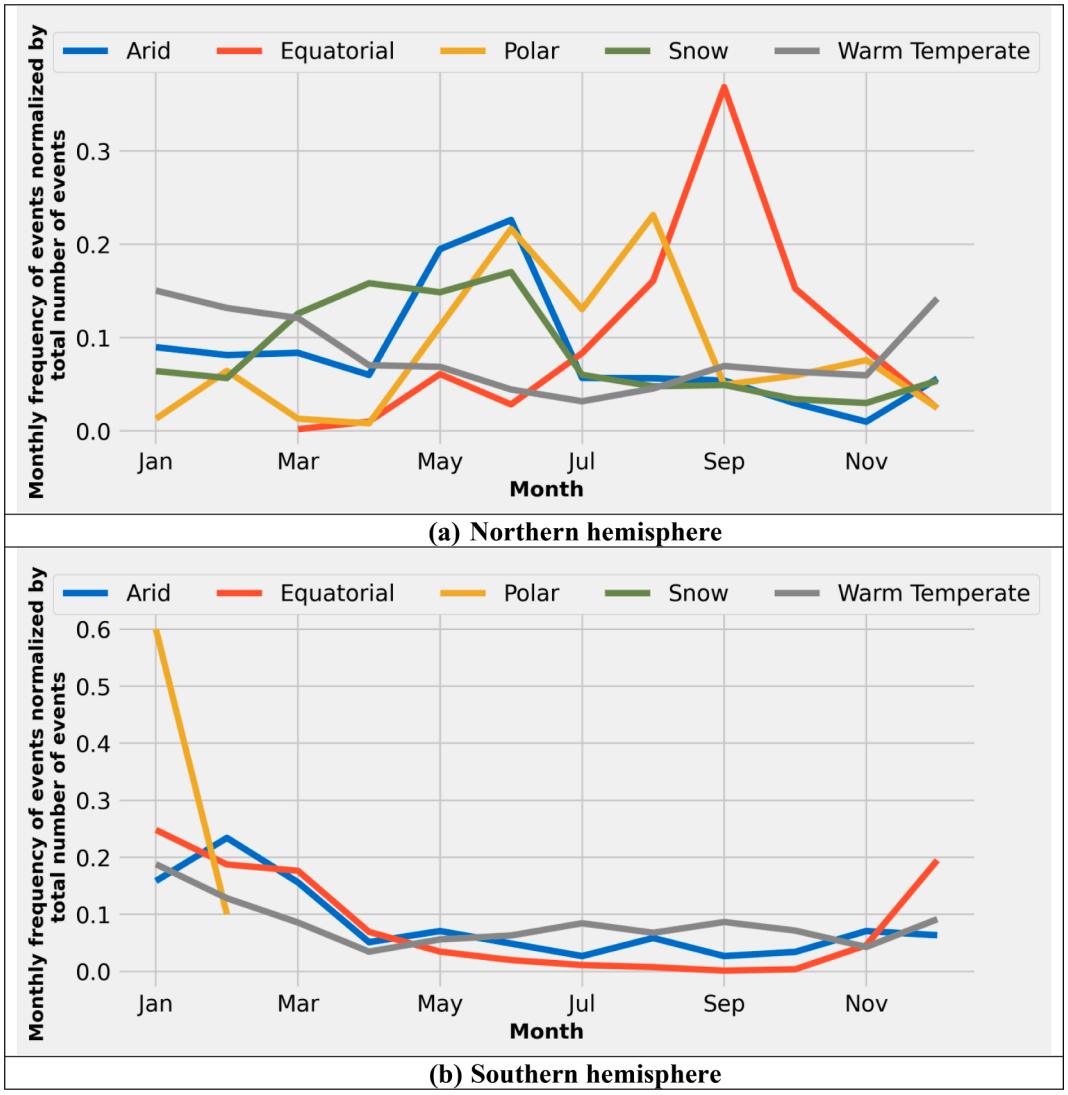

Fig. 4. Monthly distribution of high streamflow extreme (HSE) events normalized by the total number of events in different climate classes.

catchments are also mostly covered by agricultural and forest. Detailed reasoning for these characteristics is explained in subsequent sections. In comparison, the lowest unit peak discharge producing catchments were recorded in Australia. Most of them belong to the warm temperate climatic class and are dominated by unconsolidated sedimentary type lithology within their catchment boundaries. Detailed reasoning for these landcover and geologic characteristics is explained in Section 6. There is a diversity of factors that may cause high and low unit peak discharges that need to be explored. Detailed analyses and explanatory attributions are provided in the subsequent sections.

A wide variety of variables dictate the spatial differences in the magnitude of unit peak discharge across the globe. To explore the dependence of HSE on climatic regimes, the five main climatic classes (Table 1) were utilized in this study - Polar, Warm Temperate, Equatorial, Snow, and Arid. To get a quick summary of the ranges of UPDs of all the HSE events in different climatic classes, Fig. 3 displays box and whisker plots for different climatic classes. The top ten catchments in terms of high UPD values are highlighted with red color cross marks. Seven out of ten high UPDs belong to catchments with Warm Temperate climate. Moreover, the mean of all the HSE events in this group is higher than any other climate type. At the same time, the median of UPDs in the Polar climatic class is maximum. In contrast, both the mean and median of UPD are low in the case of HSE events over Arid regions. The high mean and median of the Polar class could be an artifact of the small sample of catchments (113) compared to the other climate classes (Table 1), with most of them (92) clustered in the central part of Europe spread over Switzerland, Austria, Germany, and France, which are highlighted with a yellow box in Fig. 1. This region experiences high precipitation from June to August, as shown in Fig. 1. Subsequently, the frequency of HSE events in the Polar climate dominant catchments in the northern hemisphere is high from June to August, as shown in Fig. 4(a). Besides, almost half (57) of the sample of Polar catchments are identified to have forest landcover type, and majority of them dominantly have cambisols type soil (79) and sedimentary type lithology broadly (83).

Fig. 4 shows the temporal distribution of the HSE events over different months normalized by the total number of events in different climatic classes. Since there will be a difference in seasons between the northern hemisphere (NH) and the southern hemisphere (SH) by almost 6 months, separate temporal distribution plots have been plotted for these two regions (Fig. 4(a) and (b)) resulting in rational plots on the temporal patterns of HSE events in different seasons and climatic classes. It is observed that most of the HSE events in the catchments dominated by Polar climate are observed in summer in both NH and SH. Whereas in Arid climate catchments, most of the HSE events over NH and SH are caused in May and June, and January to March, respectively. Similarly, Snow climate catchments in the NH experience most HSE events between April and June. In contrast, most of the HSE events in the catchments dominated by warm temperate climates are observed

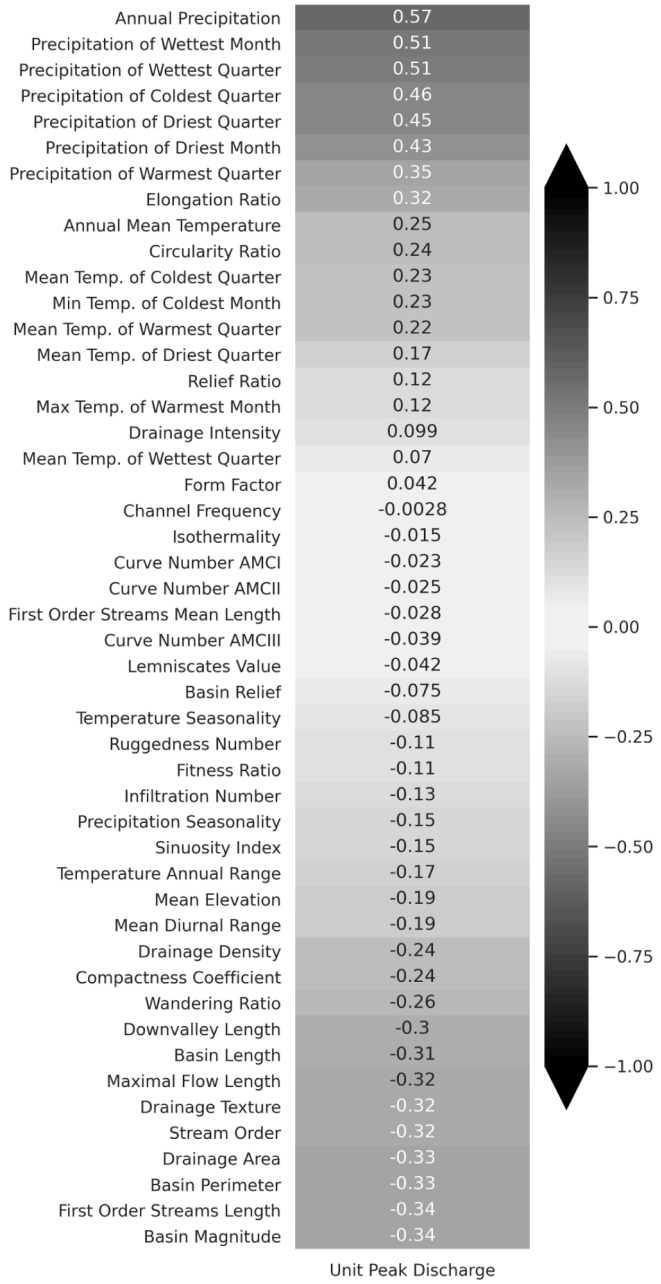

Fig. 5. Spearman-correlation coefficients between unit peak discharge of all the high streamflow events and multiple catchment characteristics. The values range from 1 to −1. The positive values represent a positive correlation, with 1 being the highest/perfect positive correlation, while the negative values represent a negative correlation, with −1 being the highest/perfect negative correlation. A value equal to 0 represents no correlation.

between December and February at NH and SH. At the same time, over Equatorial catchments in NH and SH, these extreme events are observed maximum from August to October and December to March, respectively.

4. Exploring the first-order relationship between HSE events and various geomorphological characteristics of catchments

Fig. 5 displays the spearman-correlation coefficient values between the UPD and the geomorphological, meteorological, and climatological variables. It is noteworthy that the meteorological variables display a higher correlation among other variables.

Fig. 5 reveals that geomorphological catchment characteristics such

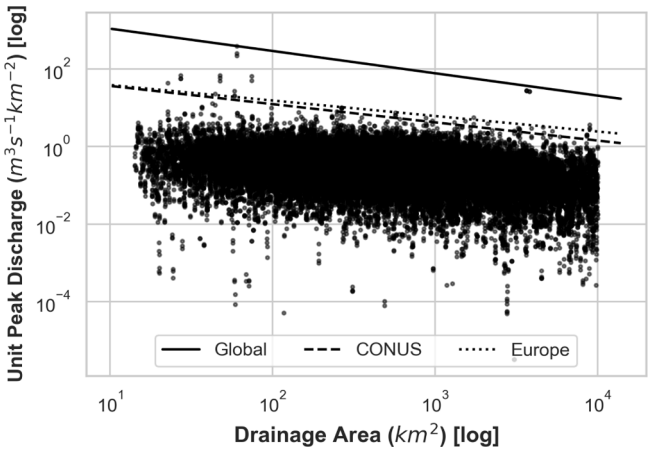

Fig. 6. Unit peak discharge vs drainage area along with their envelope curves for all the high streamflow extreme (HSE) events across the globe. The envelope curves for continental United States and Europe are taken from Marchi et al. (2010) and Saharia et al. (2017a).

as the basin magnitude, first-order streams length, basin perimeter, drainage area, stream order, and elongation ratio are highly correlated with the unit peak discharge. In addition, maximal flow length, drainage texture, and basin length also have higher correlation among the remaining geomorphological characteristics. Among the above-mentioned list of variables, except for the elongation ratio of the catchment, all are negatively correlated with the unit peak discharge. In contrast, the elongation ratio is positively correlated. Basin magnitude is the total number of first-order streams within the catchment boundary (Costa, 1987). In comparison, the first-order streams length is the sum of all these first-order streams in a catchment boundary. The first-order streams are known to be the outermost tributaries, and the overland flow of water dominates them (O'Briain, 2020). In addition, these streams flow into and feed the higher-order streams. As the length of the first-order streams increases, the streamflow takes more time to reach the higher-order streams/outlet and leads to lower UPD. The drainage area indicates the total geographical area contributing to the flow accumulation corresponding to its outlet location. In general, outlets of higher-order streams will have higher contributing drainage areas, which leads to higher streamflow travel time that results in lower unit peak discharges. Moreover, the basin perimeter, maximal flow length, and basin length increase with drainage area and stream order. Hence, an increase in these variables will lead to lower unit peak discharges. Here maximal flow length corresponds to the length along the most extended stream from the head of the channel to the outlet. Simultaneously, basin length corresponds to the most extended length of the line from a basin outlet to a point on the perimeter equidistant from the basin outlet in either direction around the perimeter (Gregory and Walling, 1968). According to Schumm (1956), the elongation ratio is the ratio between the diameter of a circle of the same area as the catchment and the maximum length of the catchment. This ratio describes the shape of the catchment. Higher ratios indicate that the corresponding catchment is circular, and the lower elongation ratio indicates that the catchment shape is elongated. Circular catchments with a higher elongation ratio are more efficient in runoff routing, and flow accumulates in less time in such catchments (Subramanya, 1984). Hence, an increase in the elongation ratio may increase the unit peak discharge. The boxplots of basin magnitude (Fig. S3(a)) and drainage area (Fig. S3(b)) for different climatic classes and their explanation are available in supplementary file. It depicts how those two relatively highly correlated geomorphological variables vary among different climate regions.

The upper envelope curve for the whole sample is shown in Fig. 6 as a solid line. The envelope curves of extreme floods in the continental US and Europe that are reported in existing literature are also plotted for

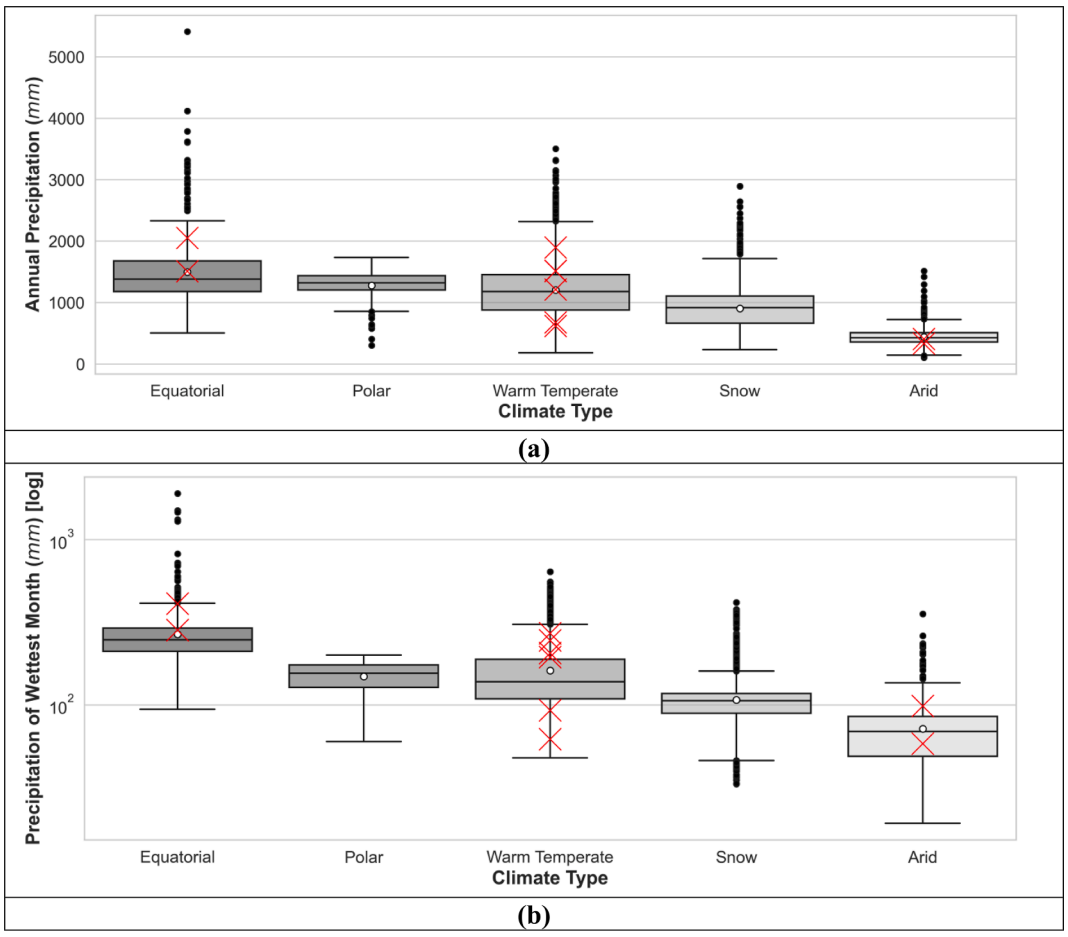

Fig. 7. Box-and-Whisker plot of (a) annual precipitation and (b) precipitation of wettest month for different climatic classes. The red cross marks correspond to the top ten catchments in terms of high unit peak discharge values. *Please refer to the caption of* Fig. 3 *for the description of the box plots.*

comparison (Gaume et al., 2009; Saharia et al., 2017a). The α and β values of the envelope curve for the global sample were estimated to be 4130.60 and −0.58. Saharia et al. (2017a) reported the α and β values for the continental United States region to be 108 and −0.47. Similar values of 97.0 and −0.40 were reported for Europe by Gaume et al. (2009). Since the deviation of β value from zero is more in the case of an envelope curve for HSE across the globe, the rate of change of unit peak discharge with the change in the drainage area is faster than continental United States and Europe catchments. Moreover, the higher α value of the global sample, when compared with values reported for the continental United States and Europe, indicates that the maximum magnitude of floods across the globe is much higher than those reported in their respective continents.

5. Exploring the first-order relationship between HSE events and various meteorological and climatological characteristics of catchments

To explore the meteorological and climatological catchment characteristics that influence HSE, the correlation between relevant variables and the magnitude of unit peak discharge is studied first. From Fig. 5, the annual precipitation has the highest correlation among all the explanatory variables available in the database, followed by precipitation of the wettest month, precipitation of wettest quarter, precipitation of coldest quarter, among other meteorological indices. As expected, all these variables are positively correlated with the unit peak discharge. Meteorological factors are considered to be the primary driver for streamflow generation across most climates (Berghuijs et al., 2019; Norbiato et al., 2009; O'Connor and Costa, 2004; Saharia et al., 2017a). The boxplot of annual precipitation for different climatic classes is plotted in Fig. 7(a). It is observed that the maximum precipitation (5413.7 mm) is recorded in a catchment belonging to the Equatorial climatic class. Equatorial has the highest mean, median, and quartile values, and it is followed by the Polar climatic class, whereas the lowest was recorded in the Arid climatic class, followed by the Snow class. Similar observations are found in the boxplot of precipitation of wettest month for different climatic classes (Fig. 7(b)). These observations explain why the Equatorial catchments can produce high unit peak discharge, as observed in Fig. 3, though the geomorphology of the same catchments is generally not favorable to produce high annual peak discharge, unlike catchments in the Polar or the Warm Temperate climatic classes. These insights also further confirm that the HSE nature is influenced by a multitude of physiographic variables.

6. Exploring the relationship between HSE events and catchment characteristics

Besides the basin characteristics related to geomorphology and climatology, other landscape variables related to soil and land cover play an important role in how precipitation is converted to runoff. In this section, we analyze how land cover, lithology, and soil type within the catchment boundary relate to the UPD of HSE and how it varies in different climates.

The dominant land cover within a catchment is expected to play a significant role in the runoff generation process and thus the unit peak discharge, as confirmed by several studies (Ahn and Merwade, 2016;

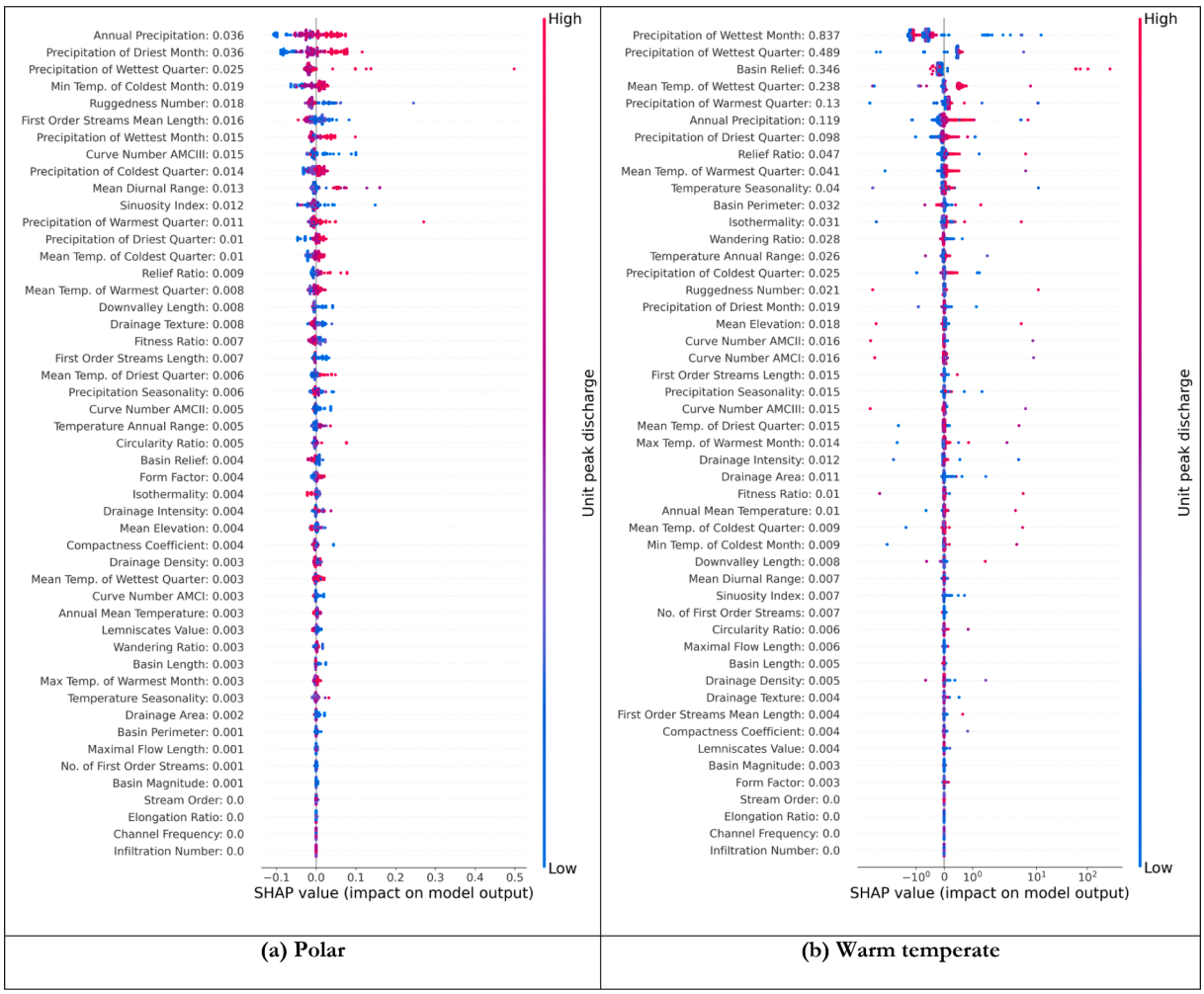

Fig. 8. SHAP summary plots for different climatic classes. The order of the features along the y-axis are based on their importance in descending order. The value on the right side of the features name along the y-axis denotes mean absolute SHAP values for the corresponding features. The horizontal location of the dots depicts the intensity of its influence on predictions. Zero values on the x-axis indicate no impact, and positive (negative) values towards the rights (left) side indicate positive (negative) impact. The color of the dots represents the values of the corresponding features if it is high (red) or low (blue) for that observation in the dataset.

Ashraf and Yasushi, 2008; Kiran et al., 2017; Woltemade et al., 2020). The change in land use and land cover alters the geomorphology of the catchment, eventually affecting floods (Cao et al., 2020). Here, we assess the impact of land cover on UPD in different climate zones. In the database, the gauge stations are classified into nine land cover types based on a dominant characteristic (covering more than 50 % catchment area). If any of the catchments do not have a dominant land cover type, they are classified as "No dominant class". The box-and-whisker plots in Fig. S4 confirm that the magnitude of the unit peak discharge varies for different land cover types across all the climates. Catchments with the greater grassland, followed by forest landcover in polar climates display considerably higher mean and median (0.631 and 0.502 $m^3s^{-1}km^{-2}$) values of UPD compared to the bare area (0.076 $m^3s^{-1}km^{-2}$), respectively. According to the Food and Agriculture Organization (FOA) of the United Nations, bare area corresponds to areas that do not have any artificial cover due to human activities and includes bare rock areas, sands, and deserts. As the sands and deserts have very high infiltration capacity, the median unit peak discharge is low in these areas. Moreover, the lithology type, soil type, and physiographic and meteorological conditions in bare areas would have a substantial impact on the magnitude of runoff generation. The catchments dominated by wetland in warm temperate (0.625 $m^3s^{-1}km^{-2}$) and arid (0.137 $m^3s^{-1}km^{-2}$) climates are observed to have high median values in those respective climates relative to other landcover dominated catchments. In contrast, wetland catchments showcase the least median (0.050 $m^3s^{-1}km^{-2}$) and mean UPD values in snow climates relative to other landcovers in the same climate. Also, permanent ice, followed by bare area and water have higher median values of UPD in snow climates. At the same time, sparse vegetation dominated catchments are observed to have the least median (0.034 $m^3s^{-1}km^{-2}$) in case of warm temperate climates and have second highest median UPD value (0.087 $m^3s^{-1}km^{-2}$) among others in case of arid climates, respectively. Subsequently, forest and grassland dominated catchments of Equatorial and warm temperate (immediately after and close to wetland and water) climates have relatively higher UPD values in their respective climate catchments. Overall, the highest median value was recorded in permanent ice landcover with 0.694 $m^3s^{-1}km^{-2}$, followed by catchments that are dominantly covered by grassland with 0.328 $m^3s^{-1}km^{-2}$, and forest with 0.318 $m^3s^{-1}km^{-2}$.

Besides, most of the top 10 catchments corresponding to the highest HSE events belong to forest and/or agriculture-dominated catchments across the climates. Agricultural practices, such as tillage, alter soil porosity and soil structure, which results in a reduction of soil infiltration rate and consequently increases surface runoff (Owuor et al., 2016). Moreover, the establishment and extension of roadside culverts, ditches, and irrigation canals in agriculture-dominated areas create new gullies

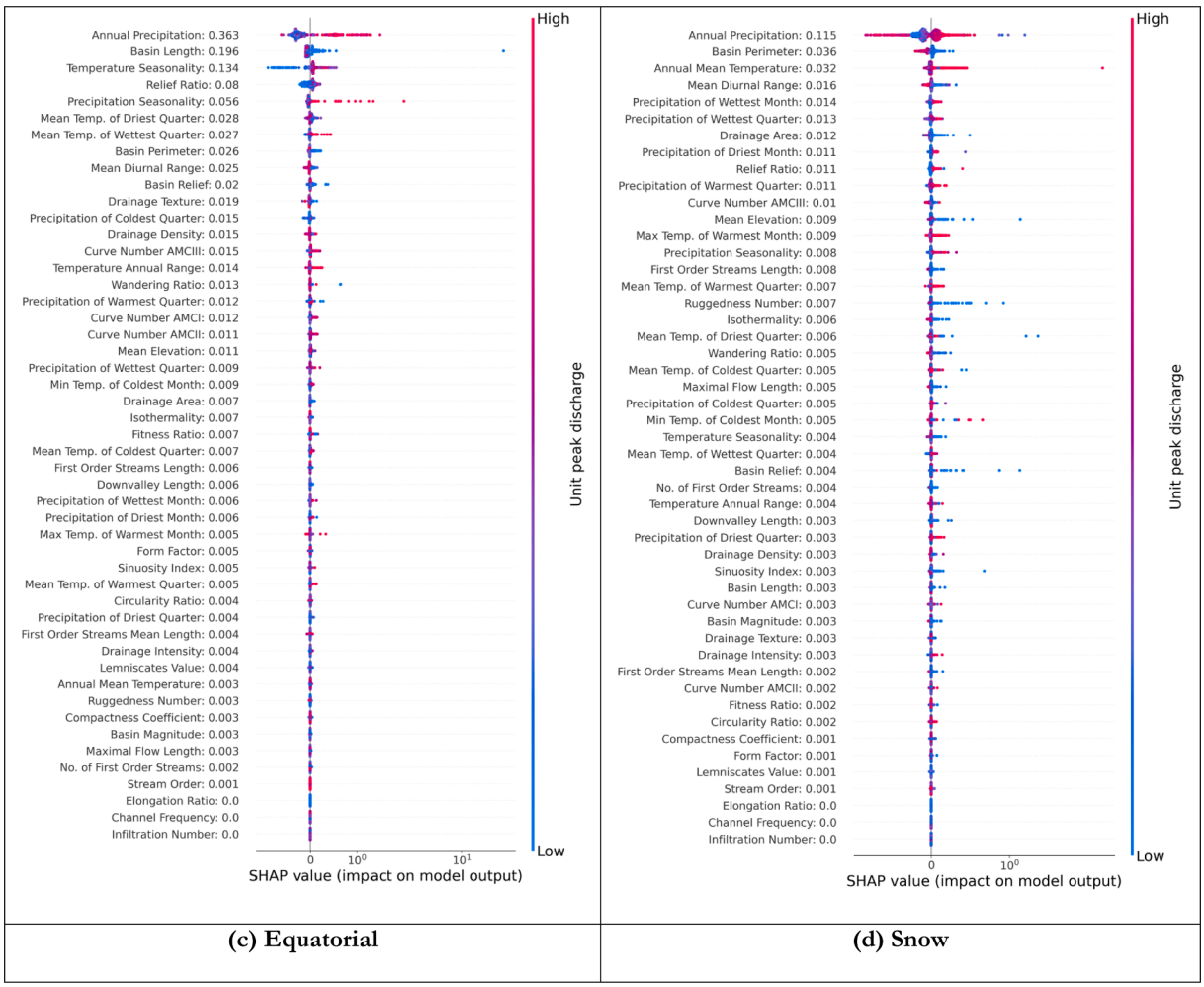

Fig. 8. (*continued*).

and channel networks (van Dijck, 2000). This phenomenon results in high stream frequency and quick overland flow of runoff in agricultural dominated catchments, and in high unit peak discharge.

Though lithology has been identified to have an impact on flooding (Gaume and Borga, 2008; Norbiato et al., 2009), very few studies have explored how the lithology of a catchment influences its magnitude. Hence the relationship between the unit peak discharge and the lithology type that is dominant (occupying more than 50 % of the area, else "No dominant type") was assessed. Box plots of unit peak discharge for different lithology types over all the main climates are plotted in Fig. S5. It is evident that the highest median values in Polar climate catchments are recorded in mixed sedimentary rocks (0.379 $m^3s^{-1}km^{-2}$), followed by acid volcanic rocks (0.379 $m^3s^{-1}km^{-2}$), and unconsolidated sediments (0.379 $m^3s^{-1}km^{-2}$). While intermediate volcanic rocks (0.379 $m^3s^{-1}km^{-2}$), followed by acid plutonic rocks (0.379 $m^3s^{-1}km^{-2}$), have significantly less median UPD values among others in the polar climates. Sedimentary rocks such as modern claystone and mudstones, composed primarily of clay minerals, have little permeability. It is also noteworthy that the thickness of regolith plays a crucial role in hydrological connectivity between the surface and the subsurface system of a catchment (Bonanno et al., 2021; Gourdol et al., 2021). Besides, as per Miyaoka et al. (1999), in some sedimentary catchments, the regolith layer is thinner than the intrusive igneous catchments. Due to the thinner regolith, runoff generation is much higher in catchments with sedimentary bedrocks than in igneous bedrock catchments when other catchment characteristics are favorable. Precipitation percolates into the fractured bedrock, mixes with soil water in the regolith, and discharges quickly into the sedimentary rock catchment (Miyaoka et al., 1999).

At the same time, intermediate volcanic rocks, followed by acid volcanic rocks in the warm temperate climate, have high median UPD values, among others. However, there is little difference in median values among each other, indicating that the lithology type has little influence on HSE in catchments with warm temperate climates.

Pyroclastics followed by basic volcanic rocks dominated catchments are observed to have high median values in equatorial climate catchments. While mixed sedimentary and unconsolidated sediments, both in the case of equatorial and warm temperate, have relatively lower median UPD values in their respective climates. In the case of ice and glaciers, basic plutonic rocks are connected to relatively high median values. Whereas intermediate volcanic rocks, followed by acid plutonic rocks and acid volcanic rocks, have high and low median values in arid climates, respectively. Basic plutonic rocks and basic volcanic rocks are igneous rocks that are also known to be primary rocks that have high unit peak discharge. Basic rocks are characterized by less silica content. Basic oxides in the basic rocks make both basic plutonic rocks and volcanic rocks much denser and more compact. Generally, water tends to flow quickly without any infiltration over these types of rocks, which may result in high median unit peak discharges. However, the hydrologic connectivity across complex structure catchments is also influenced by the interaction between soil zone water tables, deeper bedrock aquifers, and the potential spatial variability of these integrations (Jencso and McGlynn, 2011).

The infiltration capacity, soil moisture holding capacity, and other

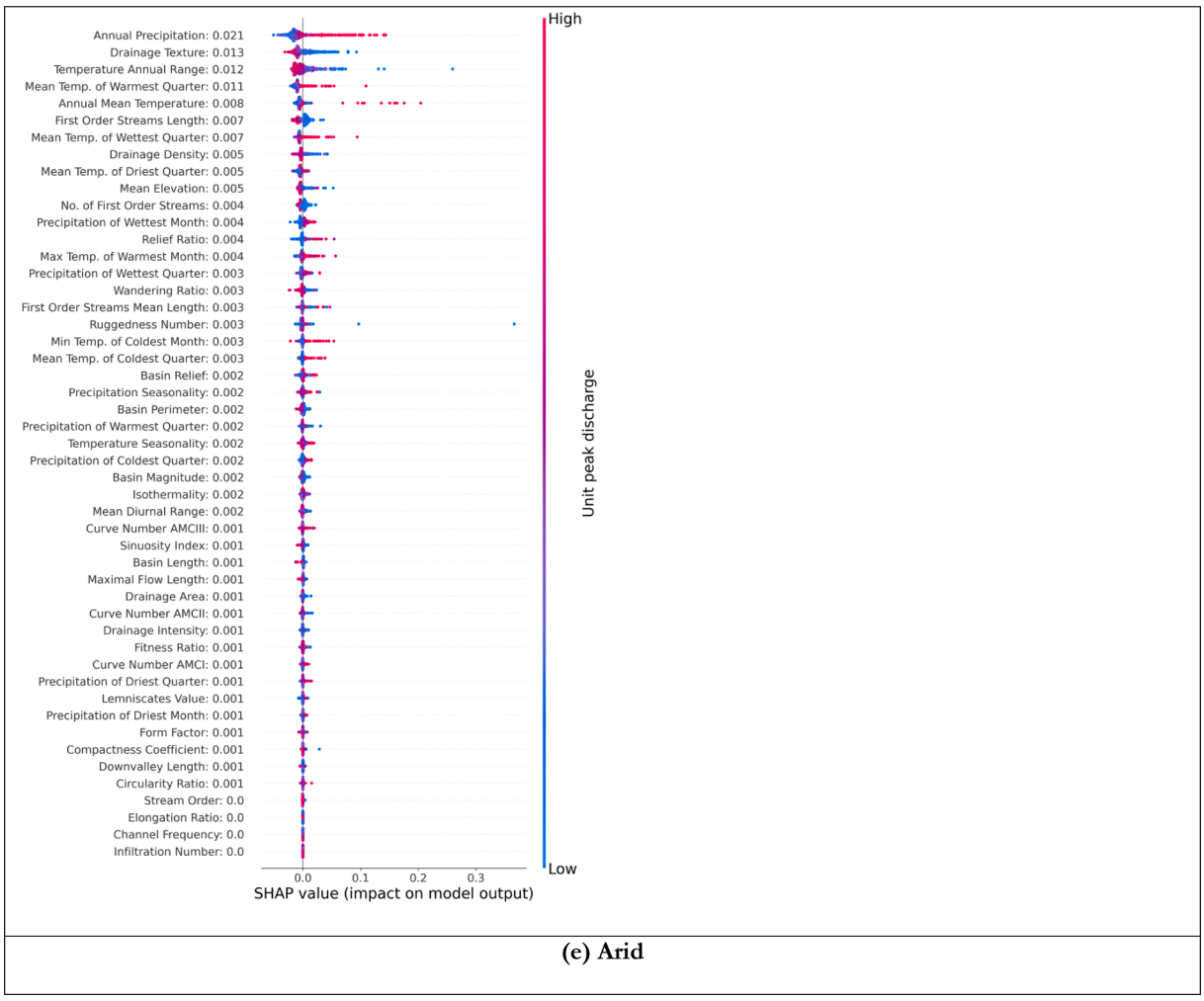

Fig. 8. (*continued*).

Table 2
Random Forest model predictions statistics.

Climate region	Statistic	Value
Polar	Accuracy	84.9 %
	Mean absolute error	0.08
Warm Temperate	Accuracy	68.37 %
	Mean absolute error	0.14
Equatorial	Accuracy	83.84 %
	Mean absolute error	0.11
Snow	Accuracy	80.88 %
	Mean absolute error	0.06
Arid	Accuracy	67.81 %
	Mean absolute error	0.04

soil properties corresponding to each soil type will impact the magnitude of streamflow or floods (Ahn and Merwade, 2016; Berghuijs et al., 2019; Ivancic and Shaw, 2015; Kuntla, 2021; Norbiato et al., 2009). Box plots of unit peak discharge for different soil types over all the climates are plotted in Figure S6. Catchments with cambisols have maximum median value in the polar climates (0.483 $m^3s^{-1}km^{-2}$). Whereas, in the warm temperate climates, high median values of UPD are observed in fluvisols, followed by podsols and nitisols dominated catchments. Nitisols allow water to drain at a moderate rate with a 30 percent clay in its subsurface horizon. These are mostly found in level to hilly land under tropical rain forests or savannah vegetation. While in arid climates, catchments dominated by vertisols possess high median UPD, followed by ferralsols. Likewise, vertisols showcase high median values in Equatorial climates. In contrast, catchments dominated by solonetz soil type had the lowest median value (0.013 $m^3s^{-1}km^{-2}$). The parent material of solonetz type soil is unconsolidated materials. Moreover, they are associated with a flatlands and steppe climate including dry summers and annual precipitation of less than 400–500 mm (Land and Water Division, 2006). Hence, catchments dominated by this soil type may have lower median unit peak discharge. Gleysols, followed by alisols dominated catchments are observed to have high median UPD values in the Snow climate. At the same time, most of the top 10 severe floods across all the climates observed to be associated with ferralsols and/or cambisols (see Fig. 8(c)). Ferralsols represent the classical soils weathered from basic rocks. These are exclusively found in Africa and South America in humid tropics and in regions in southeast Asia where the climate is hot and humid with easily weathering basic rocks (Land and Water Division, 2006). They are well-drained but have low water storage capacity. Due to their geographic locations, climate, and meteorological conditions and properties, out of the ten highest unit peak discharges, most are associated with basins recorded here.

Further comprehensive reasoning and investigation into the influence of landcover, lithology, and soil types on UPD or floods, in general, is beyond the scope of this study.

7. Relative importance of catchment characteristics on HSE

As it is observed that extreme events share a complex nonlinear relationship and are a result of an interplay between a multitude of catchment variables in the earlier sections, here in this section, we

perform a multidimensional analysis of catchment characteristics on HSE utilizing a random forest model and SHAP. The multidimensional analysis in this section is also carried out based on main climates wise, resulting in detailed insights on dominant variables in each climatic class. The accuracy statistics of the model predictions for the remaining 25 % of the events, compared with their corresponding observation values for different climatic classes, are tabulated in Table 2.

Annual precipitation, precipitation of driest month, precipitation of wettest quarter, min. temperature of coldest month and ruggedness number are observed to be the top 5 influencing features in the polar climate dominant catchments according to the SHAP summary plot (Fig. 8(a)). In addition, it confirms that annual precipitation and precipitation of driest month and wettest quarter are positively correlated, as seen in the first-order analysis of this study, with a capacity of influencing the SHAP value of UPD by ± 0.1 alone. Also, the lower values of the minimum temperature of coldest month have a negative impact on modeling UPD with more intensity compared to the positive impact of the higher values. At the same time, lower ruggedness number values have a high-intensity positive impact on the model compared to the negative impact of the higher values.

In the case of warm temperate dominated catchments, as per Fig. 8 (b), and the mean absolute value of the SHAP values, precipitation of wettest month, precipitation of wettest quarter, and basin relief are significantly top 3 dominant features over the remaining on predicatnd – UPD of HSE. Moreover, it is observed that a few events corresponding to lower values of precipitation of wettest month have a high positive impact on the model, while the intermittent distribution of both higher and lower values on the negative side confirms that there is likely another interaction at play beyond this variable, but in general as an aggregate of all events it is the most influencing variable. At the same time, lower values of the precipitation of wettest quarter corresponding to a few of the predicted target values have a higher negative impact, but overall, the distribution confirms that this variable is positively correlated with higher values having minimal impact on the target variable compared to other features and as in case of an earlier noted lower values. In the case of basin relief, the higher values have a high impact on both sides, while lower most of lower values are close to zero, having not much impact. Higher values of the mean temperature of wettest quarter have a positive impact on the model, while lower values have a negative impact, with most of them being close to zero.

At the same time, in the case of equatorial dominated catchments, annual precipitation and basin length are the top 2 influencing variables with a huge margin among others based on the absolute mean of SHAP values for modeling UPD. Moreover, Fig. 8(c) illustrates that higher values of annual precipitation have a huge positive impact on the model output. In contrast, lower basin length values have a positive impact compared to higher basin lengths, as expected.

According to the SHAP summary plot of HSE events in Snow regions, annual precipitation, basin perimeter, annual mean temperature, mean diurnal range, and precipitation of wettest month are topmost five important variables for modeling. Besides, it is observed that most of the high values of annual precipitation have a high impact in both directions showing a likelihood of another interaction at play. In comparison, basin perimeter shows an evident negative correlation with the target variable. Besides, higher annual mean temperature values have a higher positive impact on the model, and lower values do not exhibit much impact on the model. The mean absolute value of SHAP values of annual precipitation feature (0.115) is observed to be three times its consecutive variable, showing it has significant influence over the other variables among the top 5.

Finally, annual precipitation, drainage texture, temperature annual range, mean temperature of warmest quarter, and annual mean temperature are the top 5 influencing features in the arid catchments based on the SHAP summary plot as shown in Fig. 8(e). Besides, it was observed that the lower drainage texture values exhibit a high positive impact on the model compared to the intensity of its higher values on the negative side. Similarly, the temperature annual range also possesses the same characteristic in the model. In contrast, higher values of the mean temperature of warmest quarter and annual mean temperature have a positive impact on the model with great influence compared to its lower values, which have a negative impact on the model.

8. Conclusion

A database that allows for the characterization of streamflow extremes across the globe was built by using a spatially representative dataset of gauge observations combined with catchment-averaged geographical attributes. With the objective to provide a broad overview of a critical characteristic - unit peak discharge – of streamflow extremes across the world, spatial and temporal distribution plots, boxplots, correlation plots, envelop curves, and a machine learning approach (random forest model combined with SHAP) were employed whose preliminary results are summarized as follows:

- It is found that, in general, meteorological variables have a larger correlation with the UPD of HSE events compared to geomorphological variables. Among the meteorological variables, annual precipitation, precipitation of wettest month and quarter, precipitation of coldest quarter, precipitation of driest quarter and month showed the highest correlations. For geomorphology, basin magnitude, first-order streams length, basin perimeter, drainage area, stream order, drainage texture, and elongation ratio are among the variables which displayed the highest correlation with the UPD of HSE events.
- Catchments in the polar climates have high median and mean values of UPD of HSE events, followed by warm temperate. In contrast, catchments in the arid region have the lowest median and mean UPD values among catchments in other climates.
- It is observed that the UPD values of HSE events over the mountainous terrain along the oceans are usually high across the world. In contrast, the UPD values of HSE events are comparatively low on the leeward side along the mountain range. Besides, across climatic zones, many of the catchments over which high UPDs are recorded are dominated by forest and agricultural landcover in their catchments. Subsequently, a combination of catchment characteristics is associated with these catchments depicting a need in this study.
- The temporal distribution of most of the HSE events in the catchments dominated by Polar climate are observed in summer. While in Arid climate catchments, most of the HSE events over NH and SH are caused in May and June, and January to March, respectively. Similarly, Snow climate catchments in the NH experience most HSE events between April and June. Whereas, most of the HSE events in the catchments dominated by Warm temperate climates are observed between December and February at NH and SH. At the same time, over Equatorial catchments in NH and SH, these extreme events are observed maximum from August to October and December to March, respectively.
- Envelope curves over the global extremes were consistent with relationships developed over continental United States and Europe in the existing studies. Besides, the higher α value, i.e., the reduced discharge of the global sample, compared with values reported for the continental United States and Europe, indicates that the maximum magnitude of extremes across the globe is much higher than those reported in their respective catchments. Moreover, the higher deviation value of β from zero in the case of global events

indicates the rate of change of UPD with change in drainage area is faster than continental United States and Europe catchments.

- In General, catchments dominated by forests are observed to have high median values of UPD of HSE events across the world. At the same time, catchments dominated by mixed sedimentary rocks in polar climates, intermediate volcanic rocks in warm temperate climates, pyroclastics, followed by basic volcanic rocks in equatorial climates, Ice and glaciers, followed by basic plutonic type lithology in snow climates, and intermediate volcanic rocks in arid catchments have a high median value of UPD of HSE events in their respective climates among other catchments – covered with different lithology types. The maximum median value of UPD corresponds to cambisols in polar climates, fluvisols in warm temperate, vertisols in equatorial and arid, and gleysols, followed by alisols soil type dominated catchments, among others in their respective climates. These findings advise that catchments with these characteristics generally have a high UPD in their respective climates. However, since the resultant is a result of a multitude of variables, many other factors combinedly come into play. Moreover, these ambiguous observations in this study highlight the necessity for a more comprehensive study on how land features like landcover, lithology, and soil type will influence the magnitude of high streamflow extremes or floods.
- The random forest machine learning approach is relatively new in combination with the SHAP interpretable approach. It is observed that meteorological variables, especially annual precipitation, are the most influencing variable across the climatic classes leaving warm temperate where precipitation of wettest month is the top influencing one. The summary of most influencing variables in each climatic class are as follows:
  a. Polar: Annual precipitation, precipitation of driest month, precipitation of wettest quarter, min. temperature of coldest month and ruggedness number
  b. Warm Temperate: precipitation of wettest month, precipitation of wettest quarter, and basin relief.
  c. Equatorial: annual precipitation, and basin length
  d. Snow: annual precipitation, basin perimeter, annual mean temperature, mean diurnal range, and precipitation of wettest month.
  e. Arid: annual precipitation, drainage texture, temperature annual range, mean temperature of warmest quarter, and annual mean temperature.

Overall, a clear insight into the possible spectrum of unit peak discharge values is extracted from these relationships to predict the unit peak discharge at ungauged stations from the known catchment characteristics. These findings can also help assess the nature of extremes in future climate scenarios, consequently implicating risk management methods.

Future studies could employ more sophisticated modeling techniques and information-theoretic approaches to explore the relationships between basin attributes. The dataset developed as a part of this study is expected to have a wide variety of applications in land surface hydrology and encourages to development of similar datasets utilizing multiple global datasets. This study lays the groundwork for testing fundamental hydrological theories and empirical relationships by embracing data-driven science as the new paradigm in hydrology.

CRediT authorship contribution statement

Sai Kiran Kuntla: Conceptualization, Formal analysis, Data curation, Writing – original draft. **Manabendra Saharia:** Conceptualization, Methodology, Writing – review & editing. **Pierre Kirstetter:** Writing – review & editing.

Declaration of Competing Interest

The authors declare that they have no known competing financial interests or personal relationships that could have appeared to influence the work reported in this paper.

Data availability

The data that support the findings of in this study were derived from resources available in the public domain

Acknowledgements

This research was conducted in the HydroSense Lab (https://hydrosense.iitd.ac.in/) at the Indian Institute of Technology Delhi. The authors acknowledge IIT Delhi High Performance Computing facility for providing computational and storage resources. Manabendra Saharia acknowledges the financial support for this research through an ISRO Space Technology Cell grant (RP04139) and the IIT Delhi New Faculty Seed Grant. The authors would also like to thank the handling editor and the anonymous reviewers for providing useful comments which greatly improved the quality of this manuscript.

Compliance with ethical standards

The authors declare that they have no conflict of interest.

Data availability

The database that supports the findings in this study is released publicly online: Global Flood characterization (GloFlo) Database 10.5281/zenodo.7158027.

The source datasets of the same database are derived from the following resources available in the public domain:

Global Streamflow Indices and Metadata Archive (GSIM): 10.1594/PANGAEA.887477.

Global Distributed Basin Characteristics (GDBC): https://figshare.com/s/6cd00491b850bad716d7.

Worldclim: https://worldclim.org/data/worldclim21.html.

Global Kopper-Geiger Climate classification: http://koeppen-geiger.vu-wien.ac.at/present.htm.

GCN250, Global Curve Number dataset: 10.6084/m9.figshare.7756202.v1.

Global Reservoir and Dam (GRanD), version 1: https://sedac.ciesin.columbia.edu/data/set/grand-v1-dams-rev01.

Appendix

Table A1
Climate formula of Koppen-Geiger for the main climates (Kottek et al., 2006). Where, T_{max} and T_{min} are the monthly mean temperatures of the warmest and coldest months, respectively. P_{ann} is the accumulated annual precipitation. P_{th} is a dryness threshold in mm, which depends on $\{T_{ann}\}$, the absolute measure of the annual mean temperature in °C, and on the annual cycle of precipitation: $P_{th} = 2\{T_{ann}\}$ if at least 2/3 of the annual precipitation occurs in winter; $P_{th} = 2\{T_{ann}\} + 28$ if at least 2/3 of the annual precipitation occurs in summer; $P_{th} = 2\{T_{ann}\} + 14$ otherwise.

Climate	Criterion
Polar	$T_{max} < +10$ °C
Warm Temperate	-3 °C $< T_{min} < +18$ °C
Equatorial	$T_{min} \geq +18$ °C
Snow	$T_{min} \leq -3$ °C
Arid	$P_{ann} < 10\ P_{th}$

Table A2
List of all the catchment characteristics considered in this study.

Catchment Characteristics	Description	Reference
Geomorphology		
Stream order (SO)	Strahler stream order, numerical measure of river's branching complexity	(Strahler, 1952)
Drainage area (DA)	The surface area of the catchment	
Basin magnitude (B.M.)	The number of first order streams	(Melton, 1957)
First order streams length (1SL)	The total length of first order streams	(Horton, 1945)
Maximal flow length (MFL)	the length along the longest watercourse from the mouth to the head of the channel	(Mueller, 1968)
Down valley length (DVL)	The straight distance from the river cell of interest to the basin mouth	(Mueller, 1968)
Basin relief (B.R.)	The elevation difference between the highest point on the drainage divide and the mouth	(Costa, 1987)
Basin length (B.L.)	The maximal length of the line from a basin mouth to a point on the perimeter equidistant from the basin mouth in either direction around the perimeter	(Gregory and Walling, 1968)
Basin perimeter (B.P.)	The outer boundary of the watershed that enclosed its area	(Schumm, 1956)
First order streams mean length (1SML)	Mean length of first order streams. 1SML = 1SL/BM	(Strahler, 1964)
Sinuosity index (SI)	SI = MFL/DVL	(Wolman and Miller, 1960)
Form factor (FF)	$FF = DA/BL^2$	(Horton, 1945)
Relief ratio (RR)	RR = BR/BL	(Schumm, 1956)
Elongation ratio (ER)	$ER = 2/(BL \times (DA/\pi)^{0.5})$	(Schumm, 1956)
Circularity ratio (CR)	$CR = 4\ \pi\ DA/BP^2$	(Miller and Summerson, 1960)
Lemniscate value (LV)	$LV = BL^2/DA$	(Chorley, 1957)
Drainage texture (D.T.)	D.T. = Total number of streams of all order/B.P	(Horton, 1945)
Drainage density (D.D.)	D.D. = Total length of streams of all order/DA	(Horton, 1945)
Compactness coefficient (CC)	$CC = 0.2841\ (BP/DA^{0.5})$	(Gravelius, 1914)
Wandering ratio (W.R.)	MFL/BL	(Smart and Surkan, 1967)
Fitness ratio (F.R.)	MFL/BP	(Melton, 1957)
Channel frequency (CF)	CF = Total number of streams of all order/DA	(Horton, 1932)
Drainage intensity (DI)	CF/DD	(Faniran, 1968)
Infiltration number (IN)	CF × DD	(Faniran, 1968)
Ruggedness number (R.N.)	B.R. × D.D.	(Strahler, 1964)
Mean elevation (M.E.)	Mean elevation of the catchment	
Climatological/Meteorological		
Annual mean temperature (Bio1)	The annual mean temperature	(Fick and Hijmans, 2017)
Mean diurnal range (Bio2)	The mean of the monthly temperature ranges (monthly maximum minus monthly minimum)	
Isothermality (Bio3)	Isothermality quantifies how large the day-to-night temperatures oscillate relative to the summer-to-winter (annual) oscillations. Bio3= (Bio2/Bio7)x100	
Temperature seasonality (Bio4)	The amount of temperature variation over a given year (or averaged years) based on the standard deviation (variation) of monthly temperature averages.	
Maximum temperature of warmest month (Bio5)	The maximum monthly temperature occurrence over a given year (time-series) or averaged span of years (normal).	
Minimum temperature of coldest month (Bio6)	The minimum monthly temperature occurrence over a given year (time-series) or averaged span of years (normal).	
Temperature annual range (Bio7)	A measure of temperature variation over a given period. Bio7 = Bio5-Bio6	
Mean temperature of wettest Quarter (Bio8)	This quarterly index approximates mean temperatures that prevail during the wettest season.	
Mean temperature of driest quarter (Bio9)	This quarterly index approximates mean temperatures that prevail during the driest quarter.	
Mean temperature of warmest quarter (Bio10)	This quarterly index approximates mean temperatures that prevail during the warmest quarter.	
Mean temperature of coldest quarter (Bio11)	This quarterly index approximates mean temperatures that prevail during the coldest quarter.	
Annual precipitation (Bio12)	This is the sum of all total monthly precipitation values.	
Precipitation of wettest month (Bio13)	This index identifies the total precipitation that prevails during the wettest month.	
Precipitation of driest month (Bio14)	This index identifies the total precipitation that prevails during the driest month.	
Precipitation seasonality (Bio15)	This is a measure of the variation in monthly precipitation totals over the course of the year. This index is the ratio of the standard deviation of the monthly total precipitation to the mean monthly total precipitation (also known as the coefficient of variation) and is expressed as a percentage.	
Precipitation of wettest quarter (Bio16)	This quarterly index approximates total precipitation that prevails during the wettest quarter.	
Precipitation of driest quarter (Bio17)	This quarterly index approximates total precipitation that prevails during the driest quarter.	
Precipitation of warmest quarter (Bio18)	This quarterly index approximates total precipitation that prevails during the warmest quarter.	
Precipitation of coldest quarter (Bio19)	This quarterly index approximates total precipitation that prevails during the coldest quarter.	
Other catchment characteristics		
Climate type	catchment climate (major groups of Koppen-Geiger system) if one Climate type present over more than 50 % catchment area, otherwise 'No dominant class'.	(Kottek et al., 2006)
Land cover	catchment land -cover (U.N. Classification System for 2015) if one single land -cover type present over more than 50 % catchment area, otherwise 'No dominant class'.	(The Climate Change Initiative Land Cover (CCI-LC), n.d.)
Lithology type	catchment lithology if one single lithology type present over more than 50 % catchment area, otherwise 'No dominant class'.	(Hartmann and Moosdorf, 2012)
Soil type	catchment soil class (WRB) if one single soil class present over more than 50 % catchment area, otherwise 'No dominant class'.	(Hengl et al., 2017)

(*continued on next page*)

Table A2 (*continued*)

Catchment Characteristics	Description	Reference
Curve number for antecedent moisture conditions-I (dry)	An empirical parameter based on dry antecedent runoff conditions for predicting the runoff and infiltration due to a rainfall event.	(Jaafar et al., 2019)
Curve number for antecedent moisture conditions-II (average)	An empirical parameter based on average antecedent runoff conditions for predicting the runoff and infiltration due to a rainfall event.	
Curve number for antecedent moisture conditions-III (wet)	An empirical parameter based on wet antecedent runoff conditions for predicting the runoff and infiltration due to a rainfall event.	

Appendix A. Supplementary data

Supplementary data to this article can be found online at https://doi.org/10.1016/j.jhydrol.2022.128668.

References

Addor, N., Nearing, G., Prieto, C., Newman, A.J., Vine, N.L., Clark, M.P., 2018. A ranking of hydrological signatures based on their predictability in space. Water Resour. Res. 54 (11), 8792–8812. https://doi.org/10.1029/2018WR022606.

Addor, N., Do, H.X., Alvarez-Garreton, C., Coxon, G., Fowler, K., Mendoza, P.A., 2020. Large-sample hydrology: Recent progress, guidelines for new datasets and grand challenges. Hydrol. Sci. J. 65 (5), 712–725. https://doi.org/10.1080/02626667.2019.1683182.

Ahn, K.-H., Merwade, V., 2016. Role of watershed geomorphic characteristics on flooding in Indiana, United States. J. Hydrol. Eng. 21 (2), 05015021. https://doi.org/10.1061/(ASCE)HE.1943-5584.0001289.

Allaby, M. A. (2008). Bifurcation ratio. In M. Allaby (Ed.), *A Dictionary of Earth Sciences*. Oxford University Press. https://www.oxfordreference.com/view/10.1093/acref/9780199211944.001.0001/acref-9780199211944-e-868.

Al-Rawas, G.A., Valeo, C., 2010. Relationship between wadi drainage characteristics and peak-flood flows in arid northern Oman. Hydrol. Sci. J. 55 (3), 377–393. https://doi.org/10.1080/02626661003718318.

Arnell, N.W., Gosling, S.N., 2016. The impacts of climate change on river flood risk at the global scale. Clim. Change 134 (3), 387–401. https://doi.org/10.1007/s10584-014-1084-5.

Ashraf, M.D., Yasushi, Y., 2008. Effect of Land Cover Changes on Flooding: Example from Greater Dhaka of Bangladesh. Int. J. Geoinformatics 4 (1). https://creativecity-j.gscc.osaka-cu.ac.jp/IJG/article/view/604.

Berghuijs, W.R., Harrigan, S., Molnar, P., Slater, L.J., Kirchner, J.W., 2019. The relative importance of different flood-generating mechanisms across Europe. Water Resour. Res. 55 (6), 4582–4593. https://doi.org/10.1029/2019WR024841.

Blöschl, G., Hall, J., Parajka, J., Perdigão, R.A.P., Merz, B., Arheimer, B., Aronica, G.T., Bilibashi, A., Bonacci, O., Borga, M., Čanjevac, I., Castellarin, A., Chirico, G.B., Claps, P., Fiala, K., Frolova, N., Gorbachova, L., Gül, A., Hannaford, J., Živković, N., 2017. Changing climate shifts timing of European floods. Science 357 (6351), 588–590. https://doi.org/10.1126/science.aan2506.

Bonanno, E., Blöschl, G., Klaus, J., 2021. Flow directions of stream-groundwater exchange in a headwater catchment during the hydrologic year. Hydrol. Process. 35 (8), e14310.

Booker, D.J., Woods, R.A., 2014. Comparing and combining physically-based and empirically-based approaches for estimating the hydrology of ungauged catchments. J. Hydrol. 508, 227–239. https://doi.org/10.1016/j.jhydrol.2013.11.007.

Brebbia, C.A., Katsifarakis, K.L., 2007. River Basin Management IV. WIT Press.

Breiman, L., 2001. Random forests. Machine Learning 45 (1), 5–32. https://doi.org/10.1023/A:1010933404324.

Cao, W., Sofia, G., Tarolli, P., 2020. Geomorphometric characterisation of natural and anthropogenic land covers. Prog. Earth Planet. Sci. 7 (1), 2. https://doi.org/10.1186/s40645-019-0314-x.

Castellarin, A., 2007. Probabilistic envelope curves for design flood estimation at ungauged sites. Water Resour. Res. 43 (4) https://doi.org/10.1029/2005WR004384.

Chorley, R.J. (1957). Illustrating the Laws of Morphometry. Geological Magazine, 94(2), 140–150. Scopus. 10.1017/S0016756800068412.

Costa, J.E., 1987. Hydraulics and basin morphometry of the largest flash floods in the conterminous United States. J. Hydrol. 93 (3), 313–338. https://doi.org/10.1016/0022-1694(87)90102-8.

The Climate Change Initiative Land Cover *(CCI-LC)*. (n.d.). ESA/CCI Viewer. Retrieved April 15, 2022, from https://maps.elie.ucl.ac.be/CCI/viewer/.

Crippen, J.R., Bue, C.D., 1977. Maximum floodflows in the conterminous United States. Water Supply Papers - U.S, Geological Survey (USA) https://agris.fao.org/agris-search/search.do?recordID=US7759757.

Degenhardt, F., Seifert, S., Szymczak, S., 2019. Evaluation of variable selection methods for random forests and omics data sets. Briefings Bioinf. 20 (2), 492–503. https://doi.org/10.1093/bib/bbx124.

Dethier, E.N., Sartain, S.L., Renshaw, C.E., Magilligan, F.J., 2020. Spatially coherent regional changes in seasonal extreme streamflow events in the United States and Canada since 1950. Sci. Adv. https://doi.org/10.1126/sciadv.aba5939.

Do, H. X., Westra, S., Leonard, M., & Gudmundsson, L. (2020). Global-scale prediction of flood timing using atmospheric reanalysis. Water Resources Research, 56(1), e2019WR024945. 10.1029/2019WR024945.

Do, H.X., Westra, S., Leonard, M., 2017. A global-scale investigation of trends in annual maximum streamflow. J. Hydrol. 552, 28–43. https://doi.org/10.1016/j.jhydrol.2017.06.015.

Do, H.X., Zhao, F., Westra, S., Leonard, M., Gudmundsson, L., Boulange, J.E.S., Chang, J., Ciais, P., Gerten, D., Gosling, S.N., Müller Schmied, H., Stacke, T., Telteu, C.-E., Wada, Y., 2020b. Historical and future changes in global flood magnitude – evidence from a model–observation investigation. Hydrol. Earth Syst. Sci. 24 (3), 1543–1564. https://doi.org/10.5194/hess-24-1543-2020.

Dormann, C.F., Elith, J., Bacher, S., Buchmann, C., Carl, G., Carré, G., Marquéz, J.R.G., Gruber, B., Lafourcade, B., Leitão, P.J., Münkemüller, T., McClean, C., Osborne, P.E., Reineking, B., Schröder, B., Skidmore, A.K., Zurell, D., Lautenbach, S., 2013. Collinearity: A review of methods to deal with it and a simulation study evaluating their performance. Ecography 36 (1), 27–46. https://doi.org/10.1111/j.1600-0587.2012.07348.x.

Faniran, A. (1968). The index of drainage intensity—A provisional new drainage factor. *Aust J Sci*, *31*(9), 328–330. Scopus.

Fick, S.E., Hijmans, R.J., 2017. WorldClim 2: New 1-km spatial resolution climate surfaces for global land areas. Int. J. Climatol. 37 (12), 4302–4315. https://doi.org/10.1002/joc.5086.

Gaume, E., Bain, V., Bernardara, P., Newinger, O., Barbuc, M., Bateman, A., Blaškovičová, L., Blöschl, G., Borga, M., Dumitrescu, A., Daliakopoulos, I., Garcia, J., Irimescu, A., Kohnova, S., Koutroulis, A., Marchi, L., Matreata, S., Medina, V., Preciso, E., Viglione, A., 2009. A compilation of data on European flash floods. J. Hydrol. 367 (1), 70–78. https://doi.org/10.1016/j.jhydrol.2008.12.028.

Gaume, E., Borga, M., 2008. Post-flood field investigations in upland catchments after major flash floods: Proposal of a methodology and illustrations. J. Flood Risk Manage. 1 (4), 175–189. https://doi.org/10.1111/j.1753-318X.2008.00023.x.

Gourdol, L., Clément, R., Juilleret, J., Pfister, L., Hissler, C., 2021. Exploring the regolith with electrical resistivity tomography in large-scale surveys: Electrode spacing-related issues and possibility. Hydrol. Earth Syst. Sci. 25 (4), 1785–1812. https://doi.org/10.5194/hess-25-1785-2021.

Gravelius, H. (1914). *Flusskunde*. G.J. g??schen.

Gregory, K.J., Walling, D.E., 1968. The variation of drainage density within a catchment. Int. Assoc. Sci. Hydrol. Bull. 13 (2), 61–68. https://doi.org/10.1080/02626666809493583.

Gudmundsson, L., Do, H. X., Leonard, M., & Westra, S. (2018). The Global Streamflow Indices and Metadata Archive (GSIM) – Part 2: Quality control, time-series indices and homogeneity assessment. 18.

Gudmundsson, L., Leonard, M., Do, H.X., Westra, S., Seneviratne, S.I., 2019. Observed trends in global indicators of mean and extreme streamflow. Geophys. Res. Lett. 46 (2), 756–766. https://doi.org/10.1029/2018GL079725.

Gupta, H.V., Perrin, C., Blöschl, G., Montanari, A., Kumar, R., Clark, M., Andréassian, V., 2014. Large-sample hydrology: A need to balance depth with breadth. Hydrol. Earth Syst. Sci. 18 (2), 463–477. https://doi.org/10.5194/hess-18-463-2014.

Hall, J., Arheimer, B., Aronica, G.T., Bilibashi, A., Boháč, M., Bonacci, O., Borga, M., Burlando, P., Castellarin, A., Chirico, G.B., Claps, P., Fiala, K., Gaál, L., Gorbachova, L., Gül, A., Hannaford, J., Kiss, A., Kjeldsen, T., Kohnová, S., Blöschl, G., 2015. A European Flood Database: Facilitating comprehensive flood research beyond administrative boundaries. Proc. Int. Assoc. Hydrol. Sci. 370, 89–95. https://doi.org/10.5194/piahs-370-89-2015.

Hannaford, J., Marsh, T.J., 2008. High-flow and flood trends in a network of undisturbed catchments in the UK. Int. J. Climatol. 28 (10), 1325–1338. https://doi.org/10.1002/joc.1643.

Hartmann, J., & Moosdorf, N. (2012). Global Lithological Map Database v1.0 (gridded to 0.5° spatial resolution). In Supplement to: Hartmann, Jens; Moosdorf, Nils (2012): The new global lithological map database GLiM: A representation of rock properties at the Earth surface. Geochemistry, Geophysics, Geosystems, 13, Q12004, 10.1029/2012GC004370. PANGAEA. 10.1594/PANGAEA.788537.

Hengl, T., de Jesus, J.M., Heuvelink, G.B.M., Gonzalez, M.R., Kilibarda, M., Blagotić, A., Shangguan, W., Wright, M.N., Geng, X., Bauer-Marschallinger, B., Guevara, M.A., Vargas, R., MacMillan, R.A., Batjes, N.H., Leenaars, J.G.B., Ribeiro, E., Wheeler, I., Mantel, S., Kempen, B., 2017. SoilGrids250m: Global gridded soil information based on machine learning. PLoS ONE 12 (2), e0169748.

Hodgkins, G.A., Whitfield, P.H., Burn, D.H., Hannaford, J., Renard, B., Stahl, K., Fleig, A. K., Madsen, H., Mediero, L., Korhonen, J., Murphy, C., Wilson, D., 2017. Climate-driven variability in the occurrence of major floods across North America and Europe. J. Hydrol. 552, 704–717. https://doi.org/10.1016/j.jhydrol.2017.07.027.

Horton, R.E., 1932. Drainage-basin characteristics. Trans. Am. Geophys. Union 13, 350–361. https://doi.org/10.1029/TR013i001p00350.

Horton, R.E., 1945. Erosional development of streams and their drainage basins; hydrophysical approach to quantitative morphology. GSA Bulletin 56 (3), 275–370. https://doi.org/10.1130/0016-7606(1945)56[275:EDOSAT]2.0.CO;2.

Huang, Y.-F., Tsang, Y., Strauch, A.M., Clilverd, H.M., 2021. Shifting magnitude and timing of streamflow extremes and the relationship with rainfall across the Hawaiian Islands. J. Hydrol. 600, 126424 https://doi.org/10.1016/j.jhydrol.2021.126424.

Ivancic, T.J., Shaw, S.B., 2015. Examining why trends in very heavy precipitation should not be mistaken for trends in very high river discharge. Clim. Change 133 (4), 681–693. https://doi.org/10.1007/s10584-015-1476-1.

Jaafar, H.H., Ahmad, F.A., El Beyrouthy, N., 2019. GCN250, new global gridded curve numbers for hydrologic modeling and design. Sci. Data 6 (1), 145. https://doi.org/10.1038/s41597-019-0155-x.

Jencso, K.G., McGlynn, B.L., 2011. Hierarchical controls on runoff generation: Topographically driven hydrologic connectivity, geology, and vegetation. Water Resour. Res. 47 (11) https://doi.org/10.1029/2011WR010666.

Kadoya, M. (1992). Study on Record Flood Peaks in Japan. Proceedings of the Japan Academy, Series B, 68(8), 133–138. 10.2183/pjab.68.133.

Kiran, K. S., Bhuvaneswari Devi, A., & Nair, A. M. (2017, December 11). Impact of Land Use Changes in a Micro Watershed using Remote Sensing and GIS: A Case Study of IIT Guwahati Watershed, Guwahati, Assam. *7th International Ground Water Conference*.

Kottek, M., Grieser, J., Beck, C., Rudolf, B., Rubel, F., 2006. World Map of the Köppen-Geiger climate classification updated. Meteorol. Z. 259–263 https://doi.org/10.1127/0941-2948/2006/0130.

Kundzewicz, Z.W., Graczyk, D., Maurer, T., Pińskwar, I., Radziejewski, M., Svensson, C., Szwed, M., 2005. Trend detection in river flow series: 1. Annual maximum flow / Détection de tendance dans des séries de débit fluvial: 1. Débit maximum annuel. Hydrol. Sci. J. 50 (5), null-810. https://doi.org/10.1623/hysj.2005.50.5.797.

Kuntla, S.K., 2021. An era of Sentinels in flood management: Potential of Sentinel-1, -2, and -3 satellites for effective flood management. Open Geosciences 13 (1), 1616–1642. https://doi.org/10.1515/geo-2020-0325.

Land and Water Division, 2006. Guidelines for soil description. FAO. http://www.fao.org/publications/card/en/c/903943c7-f56a-521a-8d32-459e7e0cdae9/.

Latrubesse, E. M., & Brea, D. (2009). Floods in Argentina. In E. M. Latrubesse (Ed.), *Developments in Earth Surface Processes* (Vol. 13, pp. 333–349). Elsevier. 10.1016/S0928-2025(08)10016-5.

Lehner, B., Liermann, C.R., Revenga, C., Vörösmarty, C., Fekete, B., Crouzet, P., Döll, P., Endejan, M., Frenken, K., Magome, J., 2011. Global Reservoir and Dam Database. Version 1 (GRanDv1). https://sedac.ciesin.columbia.edu/data/set/grand-v1-dams-rev01.

Linsley, R.K., Kohler, M.A., Paulhus, J.L.H., 1949. *Applied Hydrology* (1st Ed Edition). McGraw Hill.

Lun, D., Viglione, A., Bertola, M., Komma, J., Parajka, J., Valent, P., Blöschl, G., 2021. Characteristics and process controls of statistical flood moments in Europe – a data-based analysis. Hydrol. Earth Syst. Sci. 25 (10), 5535–5560. https://doi.org/10.5194/hess-25-5535-2021.

Lundberg, S., & Lee, S.-I. (2017). A Unified Approach to Interpreting Model Predictions. *ArXiv:1705.07874 [Cs, Stat]*. http://arxiv.org/abs/1705.07874.

Lundberg, S.M., Erion, G., Chen, H., DeGrave, A., Prutkin, J.M., Nair, B., Katz, R., Himmelfarb, J., Bansal, N., Lee, S.-I., 2020. From local explanations to global understanding with explainable AI for trees. Nat. Mach. Intell. 2 (1), 56–67. https://doi.org/10.1038/s42256-019-0138-9.

Mallakpour, I., Villarini, G., 2015. The changing nature of flooding across the central United States. Nat. Clim. Change 5 (3), 250–254. https://doi.org/10.1038/nclimate2516.

Marchi, L., Borga, M., Preciso, E., Gaume, E., 2010. Characterisation of selected extreme flash floods in Europe and implications for flood risk management. J. Hydrol. 394 (1), 118–133. https://doi.org/10.1016/j.jhydrol.2010.07.017.

Melton, M.A., 1957. An analysis of the relations among elements of climate, surface properties, and geomorphology. Department of Geology, Columbia University, New York http://archive.org/details/analysisofrelati00melt.

Miller, O.M., Summerson, C.H., 1960. Slope-Zone Maps. Geogr. Rev. 50 (2), 194–202. https://doi.org/10.2307/211507.

Miyaoka, K., Onodera, S., Hirose, T., 1999. Effect of a permeable bedrock on runoff generation in steep mountainous catchments in the Kanto Mountains. Japan. *IAHS-AISH Publication* 23–28. http://pascal-francis.inist.fr/vibad/index.php?action=getRecordDetail&idt=1827974.

Mueller, J.E., 1968. An introduction to the hydraulic and topographic sinuosity indexes. Ann. Assoc. Am. Geogr. 58 (2), 371–385. https://doi.org/10.1111/j.1467-8306.1968.tb00650.x.

Norbiato, D., Borga, M., Merz, R., Blöschl, G., Carton, A., 2009. Controls on event runoff coefficients in the eastern Italian Alps. J. Hydrol. 375 (3), 312–325. https://doi.org/10.1016/j.jhydrol.2009.06.044.

O'Briain, R. (2020). *Eco-Hydromorphology – an emerging framework in river science* [University of Brighton]. https://cris.brighton.ac.uk/ws/portalfiles/portal/24457152/OBriain_Final.pdf.

O'Connor, J.E., Costa, J.E., 2004. Spatial distribution of the largest rainfall-runoff floods from basins between 2.6 and 26,000 km2 in the United States and Puerto Rico. Water Resour. Res. 40 (1) https://doi.org/10.1029/2003WR002247.

Owuor, S.O., Butterbach-Bahl, K., Guzha, A.C., Rufino, M.C., Pelster, D.E., Díaz-Pinés, E., Breuer, L., 2016. Groundwater recharge rates and surface runoff response to land use and land cover changes in semi-arid environments. Ecol. Process. 5 (1), 16. https://doi.org/10.1186/s13717-016-0060-6.

Pal, S., Dominguez, F., Dillon, M.E., Alvarez, J., Garcia, C.M., Nesbitt, S.W., Gochis, D., 2021. Hydrometeorological observations and modeling of an extreme rainfall event using WRF and WRF-hydro during the RELAMPAGO field campaign in Argentina. J. Hydrometeorol. 22 (2), 331–351. https://doi.org/10.1175/JHM-D-20-0133.1.

Peters-Lidard, C.D., Clark, M., Samaniego, L., Verhoest, N.E.C., van Emmerik, T., Uijlenhoet, R., Achieng, K., Franz, T.E., Woods, R., 2017. Scaling, similarity, and the fourth paradigm for hydrology. Hydrol. Earth Syst. Sci. 21 (7), 3701–3713. https://doi.org/10.5194/hess-21-3701-2017.

Project team ECA&D, & Royal Netherlands Meteorological Institute KNMI. (2013). Algorithm Theoretical Basis Document (ATBD). https://www.ecad.eu/documents/atbd.pdf.

Saharia, M., Kirstetter, P.-E., Vergara, H., Gourley, J.J., Hong, Y., 2017a. Characterization of floods in the United States. J. Hydrol. 548, 524–535. https://doi.org/10.1016/j.jhydrol.2017.03.010.

Saharia, M., Kirstetter, P.-E., Vergara, H., Gourley, J.J., Hong, Y., Giroud, M., 2017b. Mapping flash flood severity in the United States. J. Hydrometeorol. 18 (2), 397–411. https://doi.org/10.1175/JHM-D-16-0082.1.

Schumm, S.A., 1956. Evolution of drainage systems and slopes in Badlands at Perth Amboy. New Jersey. *GSA Bulletin* 67 (5), 597–646. https://doi.org/10.1130/0016-7606(1956)67[597:EODSAS]2.0.CO;2.

Seneviratne, S. I., Nicholls, N., Easterling, D., Goodess, C. M., Kanae, S., Kossin, J., Luo, Y., Marengo, J., McInnes, K., Rahimi, M., Reichstein, M., Sorteberg, A., Vera, C., Zhang, X., Rusticucci, M., Semenov, V., Alexander, L. V., Allen, S., Benito, G., … Zwiers, F. W. (2012). Changes in Climate Extremes and their Impacts on the Natural Physical Environment. In C. B. Field, V. Barros, T. F. Stocker, & Q. Dahe (Eds.), *Managing the Risks of Extreme Events and Disasters to Advance Climate Change Adaptation* (pp. 109–230). Cambridge University Press. 10.1017/CBO9781139177245.006.

Shapley, L.S., 1953. 17. A Value for n-Person Games. In: In *17. A Value for n-Person Games*. Princeton University Press, pp. 307–318. https://doi.org/10.1515/9781400881970-018.

Shen, X., Vergara, H.J., Nikolopoulos, E.I., Anagnostou, E.N., Hong, Y., Hao, Z., Zhang, K., Mao, K., 2016. GDBC: A tool for generating global-scale distributed basin morphometry. Environ. Modell. Software 83, 212–223. https://doi.org/10.1016/j.envsoft.2016.05.012.

Smart, J. S., & Surkan, A. J. (1967). The relation between mainstream length and area in drainage basins. *Water Resources Research*, *3*(4), 963–974. Scopus. 10.1029/WR003i004p00963.

Stein, L., Clark, M. P., Knoben, W. J. M., Pianosi, F., & Woods, R. A. (2021). How Do Climate and Catchment Attributes Influence Flood Generating Processes? A Large-Sample Study for 671 Catchments Across the Contiguous USA. *Water Resources Research*, *57*(4), e2020WR028300. 10.1029/2020WR028300.

Stein, L., Pianosi, F., Woods, R., 2020. Event-based classification for global study of river flood generating processes. Hydrol. Process. 34 (7), 1514–1529. https://doi.org/10.1002/hyp.13678.

Strahler, A.N., 1952. Dynamic basis of geomorphology. GSA Bulletin 63 (9), 923–938. https://doi.org/10.1130/0016-7606(1952)63[923:DBOG]2.0.CO;2.

Strahler, A.N., 1964. Quantitative Geomorphology of Drainage Basins and Channel Networks. McGraw Hill.

Subramanya, K., 1984. Engineering hydrology, 2nd ed. McGraw Hill.

Svensson, C., Kundzewicz, W.Z., Maurer, T., 2005. Trend detection in river flow series: 2. Flood and low-flow index series / Détection de tendance dans des séries de débit fluvial: 2. Séries d'indices de crue et d'étiage. Hydrol. Sci. J. 50 (5), null-824. https://doi.org/10.1623/hysj.2005.50.5.811.

van Dijck, S., 2000. Effects of agricultural land use on surface runoff and erosion in a Mediterranean area. Nederlands Geografische Studies (Netherlands). https://agris.fao.org/agris-search/search.do?recordID=NL2000003460.

Wang, S., Peng, H., Liang, S., 2022. Prediction of estuarine water quality using interpretable machine learning approach. J. Hydrol. 605, 127320 https://doi.org/10.1016/j.jhydrol.2021.127320.

Wang, F., Wang, Y., Zhang, K., Hu, M., Weng, Q., Zhang, H., 2021. Spatial heterogeneity modeling of water quality based on random forest regression and model interpretation. Environ. Res. 202, 111660 https://doi.org/10.1016/j.envres.2021.111660.

Wasko, C., Nathan, R., & Peel, M. C. (2020). Trends in Global Flood and Streamflow Timing Based on Local Water Year. Water Resources Research, 56(8), e2020WR027233. 10.1029/2020WR027233.

Winsemius, H.C., Aerts, J.C.J.H., van Beek, L.P.H., Bierkens, M.F.P., Bouwman, A., Jongman, B., Kwadijk, J.C.J., Ligtvoet, W., Lucas, P.L., van Vuuren, D.P., Ward, P.J., 2016. Global drivers of future river flood risk. Nat. Clim. Change 6 (4), 381–385. https://doi.org/10.1038/nclimate2893.

Wolman, M.G., Miller, J.P., 1960. Magnitude and frequency of forces in geomorphic processes. J. Geol. 68 (1), 54–74. https://doi.org/10.1086/626637.

Woltemade, C.J., Hawkins, T.W., Jantz, C., Drzyzga, S., 2020. Impact of changing climate and land cover on flood magnitudes in the Delaware River Basin, USA. JAWRA J. Am. Water Resour. Assoc. 56 (3), 507–527. https://doi.org/10.1111/1752-1688.12835.

Zhang, X.S., Amirthanathan, G.E., Bari, M.A., Laugesen, R.M., Shin, D., Kent, D.M., MacDonald, A.M., Turner, M.E., Tuteja, N.K., 2016. How streamflow has changed across Australia since the 1950s: Evidence from the network of hydrologic reference stations. Hydrol. Earth Syst. Sci. 20 (9), 3947–3965. https://doi.org/10.5194/hess-20-3947-2016.